THE ASTROPHYSICAL JOURNAL, 540:1016–1040, 2000 September 10

THE INITIAL MASS FUNCTION OF LOW-MASS STARS AND BROWN DWARFS IN YOUNG CLUSTERS[1,2]

K. L. LUHMAN
Harvard-Smithsonian Center for Astrophysics, 60 Garden Street, Cambridge, MA 02138; kluhman@cfa.harvard.edu

AND

G. H. RIEKE, ERICK T. YOUNG, ANGELA S. COTERA, H. CHEN, MARCIA J. RIEKE, GLENN SCHNEIDER, AND RODGER I. THOMPSON
Steward Observatory, The University of Arizona, 933 North Cherry Avenue, Tucson, AZ 85721; grieke@as.arizona.edu, eyoung@as.arizona.edu, cotera@as.arizona.edu, hchen@as.arizona.edu, mrieke@as.arizona.edu, gschneider@as.arizona.edu, rthompson@as.arizona.edu
Received 1999 December 15; accepted 2000 April 25

ABSTRACT

We have obtained images of the Trapezium Cluster (140″ × 140″; 0.3 pc × 0.3 pc) with the *Hubble Space Telescope* Near-Infrared Camera and Multi-Object Spectrometer (NICMOS). Combining these data with new ground-based K-band spectra ($R = 800$) and existing spectral types and photometry, we have constructed an H-R diagram and used it and other arguments to infer masses and ages. To allow comparison with the results of our previous studies of IC 348 and ρ Oph, we first use the models of D'Antona & Mazzitelli. With these models, the distributions of ages of comparable samples of stars in the Trapezium, ρ Oph, and IC 348 indicate median ages of $\sim$0.4 Myr for the first two regions and $\sim$1–2 Myr for the latter. The low-mass initial mass functions (IMFs) in these sites of clustered star formation are similar over a wide range of stellar densities (ρ Oph, $n = 0.2$–1×10^3 pc^{-3}; IC 348, $n = 1 \times 10^3$ pc^{-3}; Trapezium, $n = 1$–5×10^4 pc^{-3}) and other environmental conditions (e.g., presence or absence of OB stars). With current data, we cannot rule out modest variations in the substellar mass functions among these clusters. We then make the best estimate of the true form of the IMF in the Trapezium by using the evolutionary models of Baraffe et al. and an empirically adjusted temperature scale and compare this mass function to recent results for the Pleiades and the field. All of these data are consistent with an IMF that is flat or rises slowly from the substellar regime to about 0.6 $M_\odot$ and then rolls over into a power law that continues from about 1 $M_\odot$ to higher masses with a slope similar to or somewhat larger than the Salpeter value of 1.35. For the Trapezium, this behavior holds from our completeness limit of $\sim$0.02 $M_\odot$ and probably, after a modest completeness correction, even from 0.01–0.02 $M_\odot$. These data include $\sim$50 likely brown dwarfs. We test the predictions of theories of the IMF against (1) the shape of the IMF, which is not log-normal, in clusters and the field, (2) the similarity of the IMFs among young clusters, (3) the lowest mass observed for brown dwarfs, and (4) the suggested connection between the stellar IMF and the mass function of prestellar clumps. In particular, most models do not predict the formation of the moderately large numbers of isolated objects down to 0.01 $M_\odot$ that we find in the Trapezium.

Subject headings: infrared: stars — stars: evolution — stars: formation — stars: low-mass, brown dwarfs — stars: luminosity function, mass function — stars: pre–main-sequence

1. INTRODUCTION

What is the true form of the stellar initial mass function (IMF)? Is it universal, or does it depend on the properties of the natal molecular cloud or of the embedded, young stellar population? In particular, the turnover mass and the minimum mass of the IMF and their behavior with various star-forming conditions can offer vital insights into the physical processes that regulate the formation of stars and brown dwarfs (Elmegreen 1999b).

Numerous techniques have been used to measure the IMF (see reviews by Scalo 1998; Elmegreen 1999b). Stellar open clusters have played an important role, but difficulties arise in determining cluster membership and completeness at low masses, and in properly accounting for dynamical evolution and mass segregation. These problems can be alleviated in the youngest clusters ($\leq$10 Myr) associated with star-forming regions. The compact nature and thick molecular cloud of a star-forming cluster can greatly reduce contamination by foreground and background stars. Newborn substellar objects are quite luminous and should have the same spatial distribution as the stars since these regions are too young to have undergone significant dynamical evolution. Furthermore, both the initial conditions of star formation and the resulting mass function are directly observable in the youngest clusters. Stellar populations in clusters are also relevant for comparisons to the field and other regions since it is likely that clusters represent the dominant mode of star formation in the Galaxy (Lada, Strom, & Myers 1993).

The Orion Nebula Cluster centered on the Trapezium OB stars is the richest of any nearby cluster and has been studied extensively through proper motions (Jones & Walker 1988), optical images from the ground (Herbig &

[1] Based on observations made with the Multiple Mirror Telescope operated by the Smithsonian Astrophysical Observatory and the University of Arizona.

[2] Based on observations made with the NASA/ESA *Hubble Space Telescope*, obtained at the Space Telescope Science Institute, which is operated by the Association of Universities for Research in Astronomy, Inc., under NASA contract NAS 5-26555. These observations are associated with proposal ID 7217.

Terndrup 1986) and space (Prosser et al. 1994), wide-field infrared (IR) images (Ali & DePoy 1995), and high-resolution ground-based IR images (McCaughrean & Stauffer 1994, hereafter MS; Petr et al. 1998; Simon, Close, & Beck 1999). Hillenbrand (1997) combined new optical spectroscopy and photometry with previous data from the literature for more than 1000 stars within 18′ (2.5 pc) of the Trapezium OB stars and constructed a Hertzsprung-Russell (H-R) diagram for the Orion cluster. With the theoretical evolutionary models of D'Antona & Mazzitelli (1994) (hereafter DM94), she inferred an average age of less than 1 Myr and an IMF that peaked at 0.2 $M_\odot$ and fell rapidly to lower masses. Hillenbrand & Carpenter (2000) have recently extended this work to substellar masses through deep ground-based H and K imaging of the 5.′1 × 5.′1 area surrounding the Trapezium OB stars.

Within the central ~ 5 arcmin^2 of the Orion Nebula Cluster lies the Trapezium Cluster, where stellar densities reach a peak of $\sim 5 \times 10^4$ pc^{-3} (MS). Several characteristics make the Trapezium Cluster a unique region for a study of the IMF. The cluster is rich (300 stars) and nearby (450 pc) and a majority of its members have minimal extinction ($A_V < 5$) because of the cluster's location on the front of the molecular cloud and within the cavity created by the O star θ^1 Ori C. In addition, the obscuration of the molecular cloud and the compactness of the cluster minimize contamination from background and foreground stars. Because of the abrupt change in reddening from the Trapezium members to the field stars behind the cloud, virtually all sources with $A_V < 10$ should be cluster members, a crucial property in reliably identifying the substellar population. The special viewing geometry for the Trapezium Cluster overcomes many of the common limitations in correcting cluster measurements for the effects of obscuration. Consequently, it should be possible to construct an IMF from well below the hydrogen burning mass limit to about 50 $M_\odot$.

In § 2 of this paper, we describe a new study of the Trapezium Cluster. Previous observations of the low-mass population in the Trapezium have been hindered by crowding and bright nebulosity. To overcome these obstacles, we have obtained sensitive ($H \sim 17$) high-resolution (0.″2) images of the Trapezium Cluster (140″ × 140″) with the Near-Infrared Camera and Multi-Object Spectrometer (NICMOS) aboard the *Hubble Space Telescope* (*HST*). We have also measured K-band spectra for ~ 100 sources in this region. We use these measurements and data from the literature (MS; Prosser et al. 1994; Hillenbrand 1997) to construct an H-R diagram for the cluster and infer individual masses and ages from theoretical evolutionary models (D'Antona & Mazzitelli 1997, hereafter DM97; Baraffe et al. 1998, hereafter B98). The resulting star formation history is used to estimate masses for the faint sources that lack spectral types, which are combined with the masses of stars on the H-R diagram to produce a cluster IMF that reaches down to 0.01 $M_\odot$.

In § 3, we compare the Trapezium IMF with the similarly derived mass functions for the star-forming clusters IC 348 (Luhman et al. 1998, hereafter LRLL; Luhman 1999) and ρ Oph (Luhman & Rieke 1999, hereafter LR99), showing them all to be similar. Interpretation of young cluster observations is limited by the accuracy of the theoretical models for the evolution of young stars and brown dwarfs. It is now possible to mitigate this problem by testing evolutionary tracks and temperature scales against young multiple star systems that contain coeval stars of differing mass. If we use a combination of tracks (B98) and temperature scale that is closely consistent with such observational tests (see Luhman 1999), the IMF for the Trapezium and the other clusters is similar to recently determined mass functions for the Pleiades and M35 open clusters and the field. The shape of the low-mass IMF, its approximate invariance across 2 orders of magnitude in stellar density, and the presence of moderately large numbers of very low-mass brown dwarfs are used to test the predictions of various theoretical models for the origin of the IMF.

2. THE TRAPEZIUM CLUSTER

2.1. *Observations and Data Analysis*

2.1.1. *K-Band Spectroscopy*

We performed K-band spectroscopy on sources in the Trapezium Cluster using the near-IR long-slit spectrometer FSpec (Williams et al. 1993) at the Multiple Mirror Telescope on Mount Hopkins on the nights of 1995 November 8 and 10, 1995 December 2 and 3, and 1996 February 5, 6, 9, and 10. The wavelength coverage was 2.0 to 2.4 μm with a two-pixel resolution of $R = \lambda/\Delta\lambda = 800$. The observations and data reduction procedures were identical to those described by LRLL. From the K-band photometry of the central square arcminute of the Trapezium by MS, we selected for spectroscopy 64 of the 77 sources with $K < 12$ and eight sources that were somewhat fainter. In addition, we observed 29 stars with $K < 11$ appearing in images outside of the region of MS (M. McCaughrean 1996, private communication), which included several embedded sources in the BN/KL nebula (Becklin & Neugebauer 1967; Kleinmann & Low 1967). On 1996 December 28 we used a new grating that provided $R = 1200$ for follow-up observations of source n from Lonsdale et al. (1982) and the BN object (stars 50 and 44 in Table 1).

2.1.2. *NICMOS Photometry*

On 1998 January 30 we observed the Trapezium Cluster with camera 3 of NICMOS (NIC3) on *HST*. At a plate scale of 0.″201 ± 0.″001, NIC3 provides a field of view of 51.″2 × 51.″2. Nine contiguous pointings were imaged in a 3 × 3 dither pattern where the corners of the total 140″ × 140″ field have coordinates of $(\alpha, \delta)(2000) = (5^h35^m12^s.11, -5°21'48''.3)$, $(5^h35^m11^s.87, -5°24'09''.8)$, $(5^h35^m21^s.61, -5°21'51''.6)$, and $(5^h35^m21^s.37, -5°24'13''.1)$. Images were obtained through the F110W (0.8–1.4 μm) and F160W (1.4–1.8 μm) filters with integration times of 96 and 80 s, respectively. Dark frames were taken during the observations. Dark subtraction and linearity corrections were performed with the NICRED data reduction package (McLeod 1997).

Because of the number and uneven distribution of bright stars within the field of view, the background level varied considerably among the quadrants of the array and among the dithered frames. The offsets between quadrants were interactively determined by minimizing the median of the differences between border pixels. The upper right quadrant was always assumed to be correct, then the two adjacent quadrants were offset to match this quadrant. Finally, the last quadrant was adjusted to minimize the difference with the two adjacent quadrants. In constructing the mosaic images in Figures 1 and 2, offsets between the dithered frames were measured in a similar fashion. The quadrant offsets were applied prior to flat-fielding.

TABLE 1

DATA FOR THE TRAPEZIUM CLUSTER

Number	TCC[a]	ID[b]	α(2000)	δ(2000)	Previous Type[c]	IR Type[d]	Adopt	$T_{\rm eff}$	A_H	$L_{\rm bol}$	$V-I^c$	I^c	110–160	160[e]	K^f
1[g]	...	378a	5 35 12.279	−5 23 48.24	K1(H)M0(Sam)	...	K1	5080	0.60	5.9	2.11	12.89	0.98	10.03	...
2[g]	...	378b	5 35 12.279	−5 23 48.24	...	...	...	...	...	...	2.32	13.49	...	...	...
3	...	...	5 35 12.382	−5 23 51.86	...	...	...	...	...	...	...	...	2.89	14.14	...
4	...	...	5 35 12.466	−5 24 03.81	...	...	...	...	...	...	...	...	>0.6	17.63	...
5	...	9018	5 35 12.574	−5 23 02.21	...	...	...	...	...	...	4.97	17.76	2.23	11.90	...
6	...	385	5 35 12.596	−5 23 44.32	K1V(HT) < K7(P) < M0(Sam)	...	K1	5080	0.37	10	1.62	11.02	0.87	9.16	...
7	...	...	5 35 12.755	−5 21 59.22	...	...	...	...	...	...	...	...	2.55	14.63	...
8	...	...	5 35 12.772	−5 21 58.10	...	...	...	...	...	...	...	...	2.37	15.93	...
9	...	395	5 35 13.024	−5 22 01.20	M2(H)	...	M2	3510	0.52	0.33	4.05	15.32	0.90	12.40	...
10	...	9029	5 35 13.048	−5 22 15.40	M4.5(H)	...	M4.5	3095	0.21	0.47	3.28	14.21	1.19	11.55	...
11	...	9028	5 35 13.052	−5 21 53.53	...	...	...	...	...	...	3.92	17.20	1.95	12.34	...
12	...	9030	5 35 13.082	−5 22 53.36	M2:(H)	...	M1−M3	3510	0.43	0.088	3.99	16.46	0.91	13.75	...
13	...	9031	5 35 13.106	−5 22 47.32	K:(H)	...	...	...	...	...	...	15.65	1.16	14.55	...
14[g]	...	399a	5 35 13.171	−5 22 21.38	...	?	...	...	...	...	3.19	15.29	1.52	11.51	...
15[g]	...	399b	5 35 13.171	−5 22 21.38	...	...	...	...	...	...	3.88	16.77	...	...	...
16	...	...	5 35 13.229	−5 23 55.57	...	...	...	...	...	...	...	...	>2.2	17.88	...
17	...	...	5 35 13.241	−5 22 10.03	...	...	...	...	...	...	...	...	>3.8	16.30	...
18	...	...	5 35 13.252	−5 23 22.91	...	...	...	...	...	...	...	...	1.17	16.14	...
19	...	9038	5 35 13.286	−5 22 58.06	cont(H)	...	...	...	...	...	4.75	15.89	1.04	12.85	...
20	...	9037	5 35 13.312	−5 23 53.19	...	...	...	...	...	...	>3.74	17.26	0.95	14.12	...
21	...	...	5 35 13.316	−5 21 50.20	...	...	...	...	...	...	...	...	3.42	15.68	...
22	...	404	5 35 13.361	−5 22 26.41	M4.5–M5.5(H)	...	M4.5–M5.5	3010	0.15	0.29	3.38	14.65	1.30	12.00	...
23	...	9040	5 35 13.374	−5 23 53.34	...	...	...	...	...	...	>4.72	17.68	1.33	13.37	...
24	...	409	5 35 13.443	−5 23 40.41	<M0(Sam)	...	...	...	...	...	1.91	12.55	1.06	10.04	...
25	...	411	5 35 13.518	−5 22 19.80	M1.4(P)	K–M	M1–M2	3595	0.40	1.2	2.59	13.54	1.27	10.93	...
26	...	9045	5 35 13.520	−5 23 04.64	late–K:(H)	...	...	...	...	...	4.17	15.91	1.07	12.65	...
27	...	412	5 35 13.525	−5 23 31.06	M3(H)	...	M3	3350	0.17	0.42	2.83	13.98	1.11	11.68	...
28	...	...	5 35 13.542	−5 23 59.82	...	...	...	...	...	...	...	...	3.07	13.55	...
29	...	...	5 35 13.646	−5 22 11.75	...	...	...	...	...	...	...	...	0.92	16.88	...
30	...	420	5 35 13.740	−5 22 22.24	M1.5(H)	≥G6/r_K ≥ 0/CO ≥ 25	M1.5	3595	0.64	2.3	3.26	13.60	1.50	10.45	...
31	...	...	5 35 13.772	−5 22 17.65	...	...	...	...	...	...	...	...	3.56	13.14	...
32	...	...	5 35 13.799	−5 23 40.27	...	...	...	...	...	...	...	...	>2.9	17.21	...
33	...	423	5 35 13.799	−5 22 07.33	K2e(H)M0,M4(Sam)	G4–K3/r_K = 0–1	K2−K3	4815	0.62	6.8	2.10	12.30	1.31	9.76	...
34	...	...	5 35 13.800	−5 21 59.95	...	?	...	...	...	...	...	...	3.57	9.66	...
35	...	424	5 35 13.810	−5 22 03.11	...	...	...	...	...	...	3.81	15.61	1.30	12.72	...
36	...	...	5 35 13.827	−5 22 09.37	...	...	...	...	...	...	...	...	2.30	13.06	...
37	...	...	5 35 13.855	−5 23 35.05	...	...	...	...	...	...	...	...	1.24	16.35	...
38	...	...	5 35 13.924	−5 23 20.30	...	...	...	...	...	...	...	...	0.84	13.02	...
39	...	...	5 35 13.960	−5 22 32.13	...	...	...	...	...	...	...	...	2.53	13.44	...
40	...	...	5 35 13.973	−5 21 58.29	...	...	...	...	...	...	...	...	2.71	12.67	...
41	001	431	5 35 14.047	−5 23 38.60	M3(H)<M0(Sam)	...	M3	3350	0.29	2.3	2.77	12.51	0.94	9.94	9.65
42	...	...	5 35 14.053	−5 22 05.94	...	...	...	...	...	...	...	...	2.71	14.88	...
43	...	432	5 35 14.082	−5 22 36.74	M3.1(P)	K5–M2/r_K = 0–0.5/CO > 25	M2–M3	3430	0.32	1.5	3.26	13.04	1.10	10.49	...
44	...	...	5 35 14.114	−5 22 23.05	...	...	...	...	...	...	...	...	5.44	9.46	...
45	002	5176	5 35 14.162	−5 23 01.24	...	...	...	...	...	...	...	...	0.13	14.14	12.86
46	003	...	5 35 14.29	−5 23 04.44	...	...	...	...	...	...	...	...	...	...	13.45
47[g]	...	436a	5 35 14.305	−5 22 04.65	...	...	...	...	...	...	3.96	16.97	1.42	13.34	...

TABLE 1—*Continued*

Number	TCC[a]	ID[b]	α(2000)	δ(2000)	Previous Type[c]	IR Type[d]	Adopt	$T_{\rm eff}$	A_H	$L_{\rm bol}$	$V-I$[c]	I[c]	110–160	160[e]	K[f]
48[g]	...	436b	5 35 14.305	−5 22 04.65	...	...	...	...	...	...	3.79	17.52	...	...	...
49	004	9061	5 35 14.31	−5 23 08.50	mid-M:(H)	K5–M2/r_K = 0.5–1	M1–M3	3510	1.84	2.8	>4.35	17.35	...	...	10.42
50	...	...	5 35 14.351	−5 22 32.94	...	?	...	...	...	...	...	...	4.25	11.98	...
51	005	9062	5 35 14.357	−5 22 54.31	...	?	...	...	...	...	...	17.65	2.38	11.55	10.31
52	...	9063	5 35 14.363	−5 22 36.28	...	...	...	...	...	...	>4.92	18.38	2.20	12.91	...
53	006	9064	5 35 14.382	−5 22 55.99	cont(H)	...	...	...	...	...	...	18.05	1.97	13.03	11.92
54	007	441	5 35 14.395	−5 23 33.79	M1(H)	K5–M2/r_K = 0–0.5/CO > 25	M1	3680	0.32	2.1	2.58	12.61	1.36	10.23	9.33
55	...	...	5 35 14.399	−5 23 23.24	...	...	...	...	...	...	...	...	1.04	13.70	...
56	...	442	5 35 14.524	−5 22 06.98	M3(H)	...	M3	3350	0.47	0.30	3.28	15.33	1.28	12.36	...
57	008	...	5 35 14.528	−5 23 03.81	...	...	...	...	...	...	...	...	1.93	13.75	12.78
58	...	...	5 35 14.543	−5 22 51.66	...	...	...	...	...	...	...	...	2.48	16.27	...
59	...	...	5 35 14.571	−5 23 50.86	...	...	...	...	...	...	...	...	1.04	14.31	...
60	...	9066	5 35 14.617	−5 22 01.24	K:(H)	...	...	...	...	...	>5.28	17.22	1.09	13.55	...
61	...	448	5 35 14.652	−5 22 33.97	K7(P)K3–K4,M0–M1.5(Sam)	K5–M2/r_K = 0–0.5/CO > 25	K5–M1	4060	0.49	4.9	2.48	12.10	1.16	9.62	...
62	...	...	5 35 14.654	−5 23 28.86	...	...	...	...	...	...	...	...	1.14	14.20	...
63	010	9069	5 35 14.663	−5 23 02.02	M0.5–M2.5(H)	M0–M3	M0.5–M2.5	3595	0.95	1.1	3.67	15.45	2.34	11.61	11.01
64	...	...	5 35 14.678	−5 22 38.34	...	...	...	...	...	...	...	...	1.55	15.96	...
65	...	...	5 35 14.689	−5 21 56.68	...	...	...	...	...	...	...	...	>1.5	17.49	...
66	011	...	5 35 14.691	−5 22 49.65	...	K5–M2/r_K = 0.5–1	K5–M2	3955	3.07	3.9	...	...	3.21	12.55	10.94
67	...	...	5 35 14.708	−5 22 35.62	...	...	...	...	...	...	...	...	1.34	15.27	...
68	012	451	5 35 14.714	−5 23 23.09	M3e(H)	K–M	M3	3350	0.00	1.3	...	12.20	1.82	11.74	10.55
69	...	...	5 35 14.718	−5 22 29.77	...	...	...	...	...	...	...	...	>4.8	14.04	...
70	...	9073	5 35 14.806	−5 23 04.96	...	...	...	...	...	...	2.31	17.83	1.47	14.73	...
71	...	9074	5 35 14.810	−5 22 23.33	...	...	...	...	...	...	>3.89	18.21	1.00	14.79	...
72	014	453	5 35 14.819	−5 23 46.57	...	K6–M4/CO = 0–25	K6–M4	3680	0.00	1.1	...	12.30	0.98	11.95	11.93
73	013	...	5 35 14.827	−5 23 16.13	...	...	...	...	...	...	...	...	1.04	12.70	11.93
74	...	...	5 35 14.851	−5 22 44.35	...	...	...	...	...	...	...	...	>2.0	16.27	...
75	...	452	5 35 14.862	−5 22 31.83	...	...	...	...	...	...	2.96	14.61	1.33	11.73	...
76	015	9075	5 35 14.869	−5 23 05.26	...	K5–M3/r_K = 0–0.75/CO > 0	K5–M3	3850	1.41	1.8	4.82	16.38	2.12	11.60	10.34
77	016	454	5 35 14.91	−5 22 39.40	K4(H)K7(Eetal)K4–M0(Sam)	K5–M2/r_K = 0.5–1	K4–K7	4278	0.30	3.6	2.10	11.86	...	...	8.63
78	...	9081	5 35 14.923	−5 22 21.30	...	...	...	...	...	...	>3.05	19.75	1.46	16.68	...
79	017	455	5 35 14.931	−5 23 29.17	...	K–M	...	...	...	...	...	14.0	2.09	11.29	10.21
80	018	456	5 35 14.944	−5 23 39.37	...	K5–M2/r_K = 0–0.5	K5–M2	3955	0.33	3.0	2.41	12.18	1.07	9.95	9.45
81	...	457	5 35 14.99	−5 22 00.17	K3–K4(Sam)	K5–M3/r_K = 0–0.75/CO > 0	K3–K4	4660	0.38	2.6	1.96	12.53	...	...	...
82	...	9086	5 35 15.018	−5 22 31.40	M6(H)	...	M6	2840	0.06	0.12	4.16	15.62	1.08	12.98	...
83	020	...	5 35 15.032	−5 23 54.60	...	...	...	...	...	...	...	...	0.89	13.01	12.37
84	019	9085	5 35 15.035	−5 23 01.20	<M0(H)	...	...	...	...	...	3.10	17.58	1.27	14.51	13.70
85	...	...	5 35 15.066	−5 23 23.42	...	...	...	...	...	...	...	...	1.26	16.16	...
86	021	464	5 35 15.154	−5 23 46.87	...	K5–M2/r_K = 0.5–1	K5–M2	3955	0.00	0.52	...	13.00	1.30	11.72	11.11
87	022	...	5 35 15.171	−5 23 05.17	...	...	...	...	...	...	...	...	>3.2	16.66	16.10
88	023	463	5 35 15.188	−5 22 54.58	K2–K5(H)	G4–K5/r_K = 0.5–2/CO = 50	K2–K5	4660	0.57	6.8	2.14	12.12	1.30	9.57	8.56
89	...	...	5 35 15.192	−5 22 36.91	...	...	...	...	...	...	...	...	>4.4	14.38	...
90	...	467	5 35 15.199	−5 22 24.30	K7(H)	K5–M2/r_K = 0–0.5/CO > 25	K7	4060	0.33	1.3	2.15	13.06	1.41	10.94	...
91	024	...	5 35 15.204	−5 23 19.03	...	...	...	...	...	...	...	...	1.42	12.68	11.79
92	...	...	5 35 15.247	−5 23 49.94	...	...	...	...	...	...	...	...	1.38	15.85	...
93	...	9093	5 35 15.256	−5 21 56.02	...	...	...	...	...	...	>5.55	18.05	2.40	12.44	...
94	025	468	5 35 15.257	−5 22 57.08	G6–G8(H)	K0–K7/r_K = 0–1/CO = 25–100	G6–G8	5630	0.60	13	1.66	11.50	0.97	9.33	9.02
95	026	...	5 35 15.298	−5 23 23.37	...	...	...	...	...	...	...	...	1.18	13.14	12.57
96	...	470	5 35 15.32	−5 22 15.46	K3–K5(H)≤K5(P)	G4–K5/r_K = 0.5–2/CO = 50	K3–K5	4590	0.66	6.1	2.63	12.54	...	...	...

TABLE 1—*Continued*

Number	TCC[a]	ID[b]	α(2000)	δ(2000)	Previous Type[c]	IR Type[d]	Adopt	$T_{\rm eff}$	A_H	$L_{\rm bol}$	$V-I^{\rm c}$	$I^{\rm c}$	110–160	160[e]	$K^{\rm f}$
97[h]	...	9096	5 35 15.322	−5 22 25.30	...	M0–M3	M0–M3	3935	1.2	1.5	4.43	15.30	1.14	12.29	...
98	0.28	472b	5 35 15.322	−5 22 21.51	...	...	...	...	...	...	...	...	0.89[i]	10.05[i]	1600
99	0.27	...	5 35 15.347	−5 23 24.28	...	...	...	...	...	...	...	...	0.89[i]	16.05[i]	16.00
100[g,h]	...	472a	5 35 15.354	−5 23 25.62	...	...	...	...	...	...	3.28	14.84	1.39	11.03	...
101[g,h]	...	472b	5 35 15.369	−5 22 25.62	...	...	...	...	...	...	3.36	15.08	...	...	...
102	029	5177	5 35 15.376	−5 23 33.58	M2e(H)	M0–M3	M2	3510	0.31	0.69	...	...	1.14	11.39	11.01
103	...	...	5 35 15.385	−5 22 40.13	...	...	...	...	...	...	...	...	0.73	15.18	...
104	030	475	5 35 15.439	−5 23 45.63	M1e(H)	K0–K7/r_K = 0–1/CO = 25–100	M1	3680	0.32	1.6	...	12.94	1.17	10.56	9.91
105	031	476	5 35 15.478	−5 22 48.81	M2(H)	K5–M2/r_K = 0.5–1/CO > 50	M2	3510	0.52	2.1	2.70	13.34	1.25	10.42	9.86
106	032	5178	5 35 15.519	−5 23 37.56	...	K	...	...	...	...	...	...	1.27	12.35	11.30
107	033	...	5 35 15.534	−5 23 15.86	...	...	...	...	...	...	...	...	2.70	14.50	13.10
108	...	...	5 35 15.535	−5 22 46.53	...	...	...	...	...	...	...	...	>1.3	17.41	...
109	...	...	5 35 15.555	−5 22 20.40	...	...	...	...	...	...	...	...	1.34	15.93	...
110	034	...	5 35 15.556	−5 23 29.72	...	...	...	...	...	...	...	...	>2.3	15.92	13.50
111	035	9104	5 35 15.592	−5 22 59.11	...	...	...	...	...	...	4.18	15.97	1.09	12.66	12.32
112	...	480	5 35 15.613	−5 24 03.22	K8,M0(H) < M0(Sam)	...	K8–M0	3902	0.16	1.5	2.07	12.44	1.00	10.54	...
113	036	479	5 35 15.65	−5 22 56.56	G8–K1(H)	K0–K7/r_K = 0–1/CO = 25–100	G8–K1	5330	0.43	13	1.80	10.97	...	...	7.82
114	037	...	5 35 15.677	−5 23 39.24	...	K4–M2/r_K = 0.5–2/CO = 25–100	K7–M2	3765	2.98	2.6	...	...	3.16	12.84	11.15
115	038	...	5 35 15.700	−5 23 42.05	...	...	...	...	...	...	...	...	>1.3	17.00	14.40
116[k]	039	...	5 35 15.72	−5 23 22.61	...	K0–K7/r_K = 0–1/CO = 25–100	K0–K7	4660	0.91	7.3	...	...	...	...	9.31
117	041	...	5 35 15.759	−5 23 38.50	...	...	...	...	...	...	...	...	1.89	13.05	11.61
118	042	489	5 35 15.780	−5 23 26.83	...	G4–K5/r_K = 0.5–2	G4–K5	5330	0.63	2.0	...	13.7	1.45	11.36	10.02
119	040	1864	5 35 15.79	−5 23 10.13	B5–B8 + G0–G5(Par)	G4–K3/r_K = 0–1	...	13800[j]	0.00[j]	263[j]	...	8.4	...	...	6.77
120	043	...	5 35 15.80	−5 23 12.23	...	...	...	...	...	...	...	...	...	...	11.40
121	045	1865	5 35 15.83	−5 23 14.30	O9(Hp)B2(Par)B0.5V(LA) O9V(vA)B1(J)B1(S)B1.5(T)	...	...	29600[j]	0.33[j]	31600[j]	0.42	6.31	...	...	5.87
122	044	492	5 35 15.831	−5 22 46.06	M3e(H)	K6–M4/CO = 0–25	M3	3350	0.51	1.3	3.28	13.83	2.29	10.77	10.50
123[k]	046	488a	5 35 15.84	−5 23 22.70	mid-Ke(H)K1(CK)	≥G6/r_K≥0/CO≥25	K1–K3	4900	0.98	13	...	12.2	...	...	8.92
124	047	...	5 35 15.842	−5 23 25.65	...	G4–K3/r_K = 0–1	G4–K3	5465	0.74	1.3	...	...	1.55	12.01	10.97
125	049	494	5 35 15.88	−5 23 02.14	K7(H)	K4–M2/r_K = 0.5–2/CO = 25–100	...	...	...	...	2.36	13.56	...	...	9.82
126	...	9119	5 35 15.880	−5 22 33.49	M2.5:e(H)	...	M2–M3	3430	0.41	0.11	4.43	16.17	1.31	13.41	...
127	048	...	5 35 15.89	−5 23 10.93	...	...	...	...	...	...	...	...	...	...	11.40
128	050	...	5 35 15.898	−5 23 38.13	...	...	...	...	...	...	...	...	1.09	12.84	12.46
129	...	496	5 35 15.936	−5 22 21.28	K7e(H)	K–M	...	...	...	...	2.77	14.24	1.61	10.88	...
130	052	499	5 35 15.95	−5 23 50.30	K0:e(H)G5:(HT)	G4–K5/r_K = 0.5–2/CO = 50	G5–K2	5465	0.68	18	2.34	11.45	...	...	7.13
131	051	...	5 35 15.966	−5 23 22.85	...	...	...	...	...	...	...	...	1.01	14.22	13.20
132	...	...	5 35 15.995	−5 21 53.40	...	...	...	...	...	...	...	...	1.29	15.79	...
133	053	503	5 35 15.999	−5 23 53.10	F2–F7e(H)	K0–K7/r_K = 0–1/CO = 25–100	K0–K7	4660	0.60	6.2	2.16	12.33	1.13	9.71	9.07
134	054	...	5 35 16.064	−5 23 24.49	...	...	...	...	...	...	...	...	0.37	14.34	13.30
135	057	...	5 35 16.069	−5 23 27.94	...	...	...	...	...	...	...	...	1.09[i]	13.92[i]	12.90
136	056	1863b	5 35 16.07	−5 23 07.27	...	...	...	...	...	...	...	11.0	...	...	7.53
137	055	...	5 35 16.076	−5 22 54.26	...	?	...	...	...	...	...	...	3.95	13.57	11.40
138	058	...	5 35 16.096	−5 23 23.15	...	...	...	...	...	...	...	...	>1.4	16.05	13.60
139	059	...	5 35 16.097	−5 23 14.36	...	K6–M4/CO = 0–25	K6–M4	3680	0.22	0.29	...	...	1.04	12.28	11.58
140	...	...	5 35 16.102	−5 22 12.82	...	...	...	...	...	...	...	...	1.31	12.82	...
141	060	1863a	5 35 16.14	−5 23 07.21	B4(Par)B3V(LA)B0V(vA) B3(J)B3(S)B6n(T)	...	...	18700[j]	0.09[j]	1910[j]	−0.04	7.3	...	...	6.43
142	061	9128	5 35 16.140	−5 22 55.48	...	M0–M3	M0–M3	3595	1.13	0.30	>4.47	17.43	1.68	13.18	12.35
143	...	9132	5 35 16.183	−5 22 37.71	M3.5(H)	...	M3.5	3265	0.45	0.48	4.16	14.83	1.33	11.82	...

TABLE 1—*Continued*

Number	TCC[a]	ID[b]	α(2000)	δ(2000)	Previous Type[c]	IR Type[d]	Adopt	$T_{\rm eff}$	A_H	$L_{\rm bol}$	$V-I^c$	I^c	110–160	160[e]	K^f
144	...	...	5 35 16.221	−5 22 24.47	...	...	...	...	...	...	...	...	>2.9	16.44	...
145	062	...	5 35 16.23	−5 23 19.33	...	...	...	...	...	...	...	...	...	...	12.26
146	063	512	5 35 16.282	−5 23 16.73	cont(H)	K0–K7/r_K = 0–1/CO = 25–100	K0–K7	4660	0.32	2.7	...	12.3	2.22	10.31	9.55
147[g]	...	511a	5 35 16.292	−5 22 10.51	M1.5–M2e,M3–M3.5(H)	...	M1.5–M3.5	3430	0.74	0.54	3.80	15.67	1.39	12.05	...
148[g]	...	511b	5 35 16.292	−5 22 10.51	...	...	...	...	...	...	...	17.99	...	...	...
149	...	9138	5 35 16.295	−5 22 24.22	cont + emis(H)	...	...	...	...	...	>3.51	17.49	1.69	13.01	...
150	...	9140	5 35 16.302	−5 22 21.71	≥M2(H)	K–M	...	...	...	...	4.02	15.88	1.23	12.63	...
151	064	513	5 35 16.331	−5 22 49.27	M1.5e(H)	K4–M2/r_K = 0.5–2/CO = 25–100	M1.5	3595	0.65	1.4	2.94	14.15	1.32	10.99	10.57
152	...	515	5 35 16.36	−5 24 03.41	K4–K7(H) < M0(Sam)	...	K4–K7	4278	0.33	3.8	2.16	11.90	...	...	...
153	065	...	5 35 16.36	−5 23 22.49	...	...	...	...	...	...	...	...	...	...	12.20
154	066	...	5 35 16.36	−5 23 25.27	...	...	...	...	...	...	...	...	...	...	12.40
155	...	...	5 35 16.365	−5 22 22.51	...	...	...	...	...	...	...	...	2.81	15.45	...
156	...	9142	5 35 16.368	−5 21 50.93	M2.5(H)	...	M2.5	3430	0.53	0.18	4.27	16.05	1.07	13.02	...
157	067	...	5 35 16.400	−5 23 11.53	...	...	...	...	...	...	...	...	0.98	15.46	15.20
158	068	1891	5 35 16.46	−5 23 22.88	O7(Hp) < 09(H)O7(Par)O6:(LA)O7V(vA)O6(J)O9(T)O6(S)	...	...	40100[j]	0.30[j]	251000[j]	0.33	4.81	...	...	4.41
159[g]	...	519a	5 35 16.482	−5 22 35.45	M4(H)	...	M4	3180	0.41	0.77	3.47	14.30	1.15	11.26	...
160[g]	...	519b	5 35 16.482	−5 22 35.45	...	...	...	...	...	...	2.36	17.51	...	...	...
161	069	...	5 35 16.484	−5 22 56.62	...	M4–M6	M4–M6	3010	2.49	0.86	...	...	2.86	13.28	12.10
162	...	...	5 35 16.539	−5 22 53.84	...	...	...	...	...	...	...	...	1.91	16.36	...
163	...	521	5 35 16.575	−5 24 06.19	M0(H)	...	M0	3850	0.60	1.0	4.16	14.32	1.10	11.38	...
164	...	...	5 35 16.588	−5 22 50.51	...	...	...	...	...	...	...	...	–0.07	17.24	...
165[l]	070	...	5 35 16.612	−5 23 16.27	...	K5–M3/r_K = 0–0.75/CO > 0	K5–M3	3850	0.64	1.5	...	...	1.46	11.02	10.77
166	071	...	5 35 16.653	−5 23 28.99	...	...	...	...	...	...	...	...	2.62	13.95	12.60
167	072	1892	5 35 16.71	−5 23 25.33	B8(Par)	?	...	11300[j]	0.00[j]	69[j]	...	9.2	...	...	9.01
168	...	9151	5 35 16.722	−5 22 31.49	M4(H)	K–M	M4	3180	0.35	0.31	3.07	15.03	1.30	12.18	...
169[l]	073	524	5 35 16.745	−5 23 16.56	...	G4–K5/r_K = 0.5–2/CO = 50	G4–K5	5330	0.55	4.5	...	12.2	1.38	10.39	9.05
170	074	...	5 35 16.761	−5 23 28.20	...	M2–M5?	M2–M5	3265	0.28	0.37	...	...	1.10[i]	11.92[i]	10.90
171	...	...	5 35 16.763	−5 22 11.91	...	...	...	...	...	...	...	...	2.04	17.00	...
172[g]	...	526a	5 35 16.764	−5 24 04.38	K6(H)K6(Eetal)K4III(Ham)K2–K3(Sam)	...	K6	4205	0.44	6.7	1.90	11.87	1.05	9.29	...
173[g]	...	526b	5 35 16.764	−5 24 04.38	...	...	...	...	...	...	2.18	13.40	...	...	...
174	076	...	5 35 16.830	−5 23 42.38	...	...	...	...	...	...	...	...	3.09	15.08	13.20
175	077,075	...	5 35 16.843	−5 23 26.36	...	...	...	...	...	...	...	...	0.01	13.31	12.03
176	078	9153	5 35 16.859	−5 23 07.26	...	...	...	...	...	...	4.21	16.42	1.08	13.37	13.26
177	...	529	5 35 16.883	−5 22 22.65	M0(Sam)	K5–M2/r_K = 0.5–1/CO > 50	M0	3850	0.41	3.4	2.50	12.40	1.13	9.88	...
178	079	...	5 35 16.896	−5 22 55.27	...	...	...	...	...	...	...	...	1.99	13.56	12.56
179	...	...	5 35 16.897	−5 22 35.39	...	...	...	...	...	...	...	...	2.90	15.16	...
180	...	9155	5 35 16.921	−5 22 10.11	...	...	...	...	...	...	...	17.79	1.25	14.04	...
181	...	9158	5 35 16.929	−5 22 20.85	K7(H)	...	K7	4060	0.86	0.28	4.43	16.44	0.97	13.12	...
182	...	...	5 35 16.955	−5 23 59.70	...	...	...	...	...	...	...	...	1.20	15.54	...
183	080	532	5 35 16.966	−5 22 48.70	<K7(H)	K5–M2/r_K = 0–0.5/CO > 25	K5–K6	4278	0.73	0.45	3.62	15.53	1.02	12.54	11.81
184	081	533	5 35 16.972	−5 23 01.14	M0(H)	≥G6/r_K ≥ 0/CO ≥ 25	M0	3850	0.50	3.5	2.44	12.62	1.34	9.91	9.29
185	082	534	5 35 16.980	−5 23 37.21	M2e(H)	?	M2	3510	0.33	2.1	1.43	12.66	1.34	10.18	9.28
186	...	536	5 35 16.996	−5 22 33.23	K0−K2(H) < M0(Sam)	K5–M3/r_K = 0–0.75/CO > 0	K2–K4	4730	0.49	4.0	2.16	12.44	1.01	10.14	...
187	084	538	5 35 17.04	−5 23 34.64	K0–K2(H)	K0–K7/r_K = 0–1/CO = 25–100	K0–K2	5080	0.43	8.1	1.89	11.50	...	...	7.91
188	083	537	5 35 17.057	−5 23 39.88	K8e(H)	K4–M2/r_K = 0.5–2/CO = 25–100	K8	3955	0.53	1.9	...	13.35	1.30	10.67	10.05
189	...	...	5 35 17.111	−5 22 12.13	...	...	...	...	...	...	...	...	>2.9	16.35	...
190	085	539	5 35 17.114	−5 22 50.27	M4.5(H)	K6–M4/CO = 0–25	M4.5	3095	0.15	0.45	...	14.05	1.20	11.53	11.09

TABLE 1—*Continued*

Number	TCC[a]	ID[b]	α(2000)	δ(2000)	Previous Type[c]	IR Type[d]	Adopt	$T_{\rm eff}$	A_H	$L_{\rm bol}$	$V-I^c$	I^c	110–160	160[e]	K^f
191	086	...	5 35 17.12	−5 23 17.29	...	...	...	...	...	...	...	...	...	...	11.60
192	087	1889	5 35 17.22	−5 23 16.80	B1(Par)B0.5V(LA)B0Vp(vA) B1(J)B1(S)B1.5(T)	...	...	26300[j]	0.31[j]	22400[j]	0.40	6.30	...	...	5.85
193	...	...	5 35 17.323	−5 22 21.35	...	...	...	...	...	...	...	...	3.37	15.28	...
194	088	9178	5 35 17.325	−5 23 41.54	...	K–M	...	...	...	...	...	17.76	1.23	13.17	12.28
195	...	548	5 35 17.340	−5 22 35.95	≤K5(H) ≤ K5(P) <M0(Sam)cont+emis(CK)	G4–K5/r_K = 0.5–2	G4–K5	5330	1.50	23	2.38	13.91	1.37	9.62	...
196	090	9175	5 35 17.363	−5 23 05.03	M4–M6(H)	M4–M6?	M4–M6	3010	0.60	0.18	...	16.64	1.03	12.98	12.45
197	089	...	5 35 17.367	−5 22 45.96	...	...	...	...	...	...	...	...	3.03	14.49	12.64
198	...	...	5 35 17.379	−5 22 03.89	...	...	...	...	...	...	...	...	>4.2	15.51	...
199	...	549	5 35 17.380	−5 24 00.41	K2–K7(H)–PCygni-Paschen lines	G4–K5/r_K = 0.5–2	K2–K5	4660	1.25	3.1	3.57	15.22	1.86	11.13	...
200	091	...	5 35 17.411	−5 23 41.96	...	...	...	...	...	...	...	...	0.92	14.85	13.91
201	093	9180	5 35 17.461	−5 23 21.23	K7–K8e(H)	K0–K7/r_K = 0–1/CO = 25–100	K7–K8	3955	0.67	3.1	2.54	13.28	1.33	10.28	9.67
202	092	9181	5 35 17.470	−5 22 51.50	...	K5–M2/r_K = 0–0.5/CO > 25	K5–M2	3955	0.60	0.32	3.21	15.50	1.32	12.66	11.92
203	...	...	5 35 17.533	−5 22 00.50	...	...	...	...	...	...	...	...	>2.0	16.71	...
204	...	...	5 35 17.540	−5 23 55.20	...	...	...	...	...	...	...	...	1.61	15.05	...
205[g]	094	553a	5 35 17.553	−5 22 56.98	K3–K4(H)	≥G6/r_K ≥ 0/CO ≥ 25	K3–K4	4660	0.64	7.1	2.50	12.41	1.24	9.60	9.08
206[g]	...	553b	5 35 17.553	−5 22 56.98	...	...	...	...	...	...	1.92	14.93	...	...	...
207	095	554	5 35 17.556	−5 23 25.01	...	≥G6/r_K ≥ 0/CO ≥ 0	K0–K6	4730	0.27	0.59	...	13.8	1.53	11.98	10.62
208	...	...	5 35 17.559	−5 22 28.02	...	...	...	...	...	...	...	...	1.04	16.18	...
209	...	...	5 35 17.570	−5 24 09.17	...	...	...	...	...	...	...	...	2.01	13.74	...
210	...	...	5 35 17.599	−5 21 54.14	...	M0–M3	M0–M3	3595	1.53	0.96	...	...	2.20	12.34	...
211	...	...	5 35 17.603	−5 22 12.77	...	...	...	...	...	...	...	...	>3.6	15.10	...
212	096	9188	5 35 17.644	−5 22 51.86	...	K5–M2/r_K = 0.5–1	K5–M2	3955	0.69	0.29	3.73	15.93	1.73	12.88	11.69
213	...	9187	5 35 17.644	−5 22 08.14	≥M2(H)	...	...	...	...	...	4.34	16.21	1.16	12.84	...
214	...	...	5 35 17.658	−5 22 27.60	...	...	...	...	...	...	...	...	1.06	16.56	...
215	097	558	5 35 17.678	−5 23 41.14	<K6(H)	K–M	...	...	...	...	2.56	15.73	0.63	12.95	11.96
216	098	9194	5 35 17.721	−5 23 15.05	...	...	...	...	...	...	...	16.34	1.10	13.29	12.55
217	...	9197	5 35 17.741	−5 22 31.21	...	M2–M5?	M2−M5	3265	2.16	1.6	...	19.17	2.98	12.29	...
218	...	...	5 35 17.741	−5 23 41.33	...	...	...	...	...	...	...	...	1.03	15.99	...
219	099	9195	5 35 17.768	−5 23 42.74	...	M4–M6	M4–M6	3010	1.08	0.38	...	17.43	1.77	12.68	11.68
220	100	9196	5 35 17.782	−5 23 44.37	...	M3–M5	M3–M5	3180	0.56	0.36	4.38	15.55	1.20	12.23	11.63
221	...	...	5 35 17.810	−5 22 19.87	...	...	...	...	...	...	...	...	>2.8	16.23	...
222	101	562	5 35 17.813	−5 23 15.74	M0(H)	K5–M2/r_K = 0.5–1/CO > 50	M0	3850	0.47	2.3	2.67	13.01	1.19	10.35	9.88
223	102	...	5 35 17.835	−5 22 58.33	...	...	...	...	...	...	...	...	1.53	15.24	14.10
224	103	9201	5 35 17.862	−5 23 03.30	K8(H)	K4–M2/r_K = 0.5–2/CO = 25–100	K8	3955	0.67	1.1	2.43	14.41	1.24	11.40	10.73
225	...	...	5 35 17.868	−5 22 03.15	...	?	...	...	...	...	...	...	3.57	12.75	...
226	...	...	5 35 17.885	−5 21 53.66	...	...	...	...	...	...	...	...	3.64	14.14	...
227	104	567	5 35 17.92	−5 22 45.37	late–G(H)K3–4(HT) K4III(Ham)K2–K3(Sam)	K5–M2/r_K = 0.5–1/CO > 50	K4–K5	4470	0.21	21	1.73	9.66	...	...	7.65
228	...	...	5 35 17.961	−5 23 53.71	...	...	...	...	...	...	...	...	0.95	16.35	...
229[g]	105	9206	5 35 17.961	−5 23 35.63	...	K6–M4/CO = 0–25	K6–M4	3680	0.60	0.42	4.75	16.18	1.08	12.28	11.53
230[g]	...	9208	5 35 17.961	−5 23 35.63	...	...	...	...	...	...	4.19	15.93	...	...	...
231	...	...	5 35 18.010	−5 22 18.37	...	...	...	...	...	...	...	...	1.33	17.24	...
232	...	9209	5 35 18.015	−5 22 05.65	M0:(H)	K5–M2/r_K = 0.5–1	K7–M1	3850	1.40	4.8	3.76	15.30	1.89	10.54	...
233	...	9210	5 35 18.033	−5 24 03.27	M1(H)	...	M1	3680	1.70	8.8	5.53	15.65	2.36	10.14	...
234	106	9211	5 35 18.041	−5 23 30.96	...	K–M	...	...	...	...	>2.49	16.91	0.71	14.14	12.70
235	...	575	5 35 18.064	−5 24 01.34	...	...	...	...	...	...	3.60	14.30	1.17	11.32	...
236	107	...	5 35 18.067	−5 23 02.04	...	...	...	...	...	...	...	...	1.20	15.32	14.50

TABLE 1—*Continued*

Number	TCC[a]	ID[b]	α(2000)	δ(2000)	Previous Type[c]	IR Type[d]	Adopt	$T_{\rm eff}$	A_H	$L_{\rm bol}$	$V-I^c$	I^c	110–160	160[e]	K^f
237	...	...	5 35 18.079	−5 22 47.33	...	...	...	...	...	...	...	...	1.44	15.10	...
238	109	581	5 35 18.18	−5 23 35.74	early–Ke(H)<M0(Sam)	G4–K3/r_K = 0–1	K0–K3	4990	0.62	13	2.35	11.58	...	...	7.82
239	108	9214	5 35 18.189	−5 23 31.71	M0(H)	K–M	M0	3850	1.24	0.43	3.63	17.37	1.66	12.98	12.27
240	...	9215	5 35 18.202	−5 23 46.43	...	...	...	...	...	...	...	18.91	1.06	15.25	...
241	...	...	5 35 18.217	−5 22 06.48	...	...	...	...	...	...	...	...	3.20	14.20	...
242	110	582	5 35 18.234	−5 23 15.78	M2(H)	K5–M3/r_K = 0–0.75/CO > 0	M2	3510	0.96	1.8	3.69	14.96	1.41	11.04	10.40
243	111	9220	5 35 18.268	−5 23 07.65	M4(H)	M4–M5	M4–M5	3095	0.42	0.25	4.60	15.59	1.09	12.45	11.79
244	...	588	5 35 18.325	−5 24 05.01	M3(H)	...	M3	3350	0.37	0.13	3.54	15.92	1.54	13.18	...
245	...	589	5 35 18.36	−5 22 37.64	K0(H)G8–K0:(HT) K1IV(Ham)M0(Eetal)	K5–M2/r_K = 0.5–1/CO > 50	K3–K5	4590	0.43	9.5	2.12	11.30	...	...	...
246	...	...	5 35 18.384	−5 22 40.33	...	...	...	...	...	...	...	...	2.91	15.27	...
247	...	9228	5 35 18.463	−5 24 07.16	M3e(H)	...	M3	3350	0.42	0.95	3.14	13.91	1.04	11.05	...
248	112	9230	5 35 18.488	−5 23 29.50	M0(H)	K–M	M0	3850	0.81	0.44	5.10	15.95	1.33	12.52	12.10
249	...	9229	5 35 18.501	−5 23 57.90	...	...	...	...	...	...	...	19.13	1.68	14.51	...
250	113	...	5 35 18.517	−5 22 58.23	...	...	...	...	...	...	...	...	2.84	15.12	13.60
251	...	...	5 35 18.522	−5 23 47.96	...	...	...	...	...	...	...	...	1.17	16.86	...
252	...	9231	5 35 18.571	−5 22 31.13	cont(H)	...	...	...	...	...	>5.93	17.87	1.30	14.23	...
253	114	596	5 35 18.67	−5 23 14.35	K2–K5e(H)	?	K2–K5	4660	0.63	3.4	2.52	13.06	...	...	7.43
254	116	9232	5 35 18.672	−5 23 56.57	M2(H)	M0–M3	M2	3510	0.55	0.30	3.54	15.53	1.30	12.54	12.19
255	...	598b	5 35 18.674	−5 22 56.22	...	...	...	...	...	...	...	16.69	1.35	13.08	...
256	...	...	5 35 18.691	−5 24 02.02	...	...	...	...	...	...	...	...	1.10	17.23	...
257	115	598a	5 35 18.696	−5 22 57.05	K0–K3,K1–K5,K6(H)	≥G6/r_K ≥ 0/CO ≥ 0	K0–K6	4730	0.82	6.3	2.70	13.05	1.38	9.99	8.88
258	...	600	5 35 18.749	−5 22 02.41	M2.5(H)	K5–M2/r_K = 0.5–1/CO > 50	M2.5	3430	0.61	1.2	3.23	14.22	1.54	11.02	...
259[g]	...	9241	5 35 18.828	−5 22 23.20	M3(H)	K5–M3/r_K = 0–0.75/CO > 0	M3	3350	0.95	0.51	3.54	16.77	1.73	12.28	...
260[g]	...	9239	5 35 18.828	−5 22 23.20	...	...	...	...	...	...	...	17.54	...	...	...
261	118	...	5 35 18.865	−5 23 07.32	...	...	...	...	...	...	...	...	2.39	14.81	13.60
262	117	604	5 35 18.868	−5 23 29.05	M0e(H)	K4–M2/r_K = 0.5–2/CO = 25–100	M0	3850	0.86	0.91	3.54	15.30	1.49	11.77	10.89
263	...	9243	5 35 18.941	−5 22 18.94	K7(H)	K5–M2/r_K = 0–0.5	K7	4060	1.27	3.7	3.63	14.99	1.77	10.75	...
264	...	...	5 35 18.961	−5 23 22.12	...	...	...	...	...	...	...	...	1.15	13.65	...
265	...	...	5 35 19.028	−5 22 50.86	...	...	...	...	...	...	...	...	1.47	15.14	...
266	120	607	5 35 19.062	−5 23 49.78	G8–K2(H) ≤ K5(P)	≥G6/r_K ≥ 0/CO ≥ 0	G8–K2	5250	0.58	1.8	1.86	13.64	1.36	11.34	10.29
267	119	...	5 35 19.066	−5 23 07.70	...	...	...	...	...	...	...	...	3.88	14.97	13.06
268	121	9246	5 35 19.108	−5 23 06.48	...	...	...	...	...	...	...	18.15	1.54	14.01	13.39
269	122	610	5 35 19.113	−5 23 27.18	K8(H)	K5–M2/r_K = 0.5–1	K8	3955	0.44	0.88	2.70	13.89	1.31	11.40	10.62
270	...	9249	5 35 19.131	−5 22 34.75	...	...	...	...	...	...	>5.18	17.22	1.40	13.36	...
271	123	9250	5 35 19.204	−5 22 50.88	K5(H)	K5–M2/r_K = 0–0.5	K5	4350	0.87	2.3	2.80	14.23	1.47	10.94	10.45
272	...	...	5 35 19.375	−5 23 06.60	...	...	...	...	...	...	...	...	2.81	14.34	...
273	...	617	5 35 19.453	−5 22 21.89	≥M6(H)	...	...	...	...	...	4.41	16.58	1.51	13.10	...
274	...	...	5 35 19.495	−5 23 39.92	...	...	...	...	...	...	...	...	1.22	17.11	...
275	...	620	5 35 19.603	−5 23 57.43	K8(H)	...	K8	3955	0.42	0.51	2.59	14.41	1.06	11.97	...
276	...	...	5 35 19.620	−5 23 03.76	...	...	...	...	...	...	...	...	2.43	14.04	...
277	...	...	5 35 19.664	−5 22 34.33	...	...	...	...	...	...	...	...	1.52	15.65	...
278	...	624	5 35 19.810	−5 22 21.77	late–M(H)	?	...	...	...	...	2.88	15.44	1.79	11.97	...
279	...	...	5 35 19.841	−5 23 51.68	...	...	...	...	...	...	...	...	1.05	15.45	...
280	...	...	5 35 19.883	−5 22 07.50	...	...	...	...	...	...	...	...	1.86	14.89	...
281	...	9256	5 35 19.917	−5 24 02.74	M2(H)	...	M2	3510	0.36	0.20	4.26	15.34	1.31	12.79	...
282	...	...	5 35 19.948	−5 21 54.18	...	...	...	...	...	...	...	...	3.37	13.50	...
283	...	9257	5 35 19.964	−5 22 32.90	...	...	...	...	...	...	...	18.31	1.38	14.08	...
284	...	...	5 35 19.987	−5 23 28.94	...	...	...	...	...	...	...	...	0.72	17.15	...

TABLE 1—*Continued*

Number	TCC[a]	ID[b]	α(2000)	δ(2000)	Previous Type[c]	IR Type[d]	Adopt	$T_{\rm eff}$	A_H	$L_{\rm bol}$	$V-I^{\rm c}$	$I^{\rm c}$	110–160	160[e]	K[f]
285.....	...	630	5 35 20.017	−5 22 26.57	M5(H)	...	M5	3010	0.63	0.25	4.31	16.38	1.50	12.65	...
286.....	...	...	5 35 20.119	−5 23 04.62	...	...	...	...	...	...	...	...	1.95	16.54	...
287.....	...	9261	5 35 20.142	−5 22 28.44	...	...	...	...	...	...	4.96	16.85	1.43	12.89	...
288.....	...	3075	5 35 20.171	−5 23 08.68	...	...	...	...	...	...	...	...	1.74	11.59	...
289.....	...	645	5 35 20.38	−5 22 13.80	mid-K(H)	K5–M2/r_K = 0–0.5	K4–K7	4278	0.72	2.9	3.03	13.49	...	...	...
290.....	...	648b	5 35 20.412	−5 23 29.81	...	...	...	...	...	...	4.47	14.62	1.24	11.58	...
291.....	...	648a	5 35 20.457	−5 23 29.93	M0(H)	...	M0	3850	0.49	2.1	2.58	13.15	1.22	10.46	...
292.....	...	9264	5 35 20.493	−5 23 31.26	...	...	...	...	...	...	5.43	16.92	1.16	13.74	...
293.....	...	9266	5 35 20.505	−5 23 23.13	...	...	...	...	...	...	...	17.65	1.94	13.53	...
294.....	...	656	5 35 20.619	−5 22 55.85	M:(H)	...	...	...	...	...	4.24	17.27	1.67	12.90	...
295.....	...	...	5 35 20.626	−5 22 41.37	...	...	...	...	...	...	...	...	1.56	16.06	...
296.....	...	657	5 35 20.629	−5 22 45.74	M1(H)	...	M1	3680	1.03	0.74	3.68	16.12	1.55	12.13	...
297.....	...	659	5 35 20.664	−5 23 53.35	...	...	...	...	...	...	4.15	14.03	1.16	11.10	...
298.....	...	9270	5 35 20.700	−5 22 31.64	...	...	...	...	...	...	4.49	16.18	1.67	12.27	...
299.....	...	...	5 35 20.757	−5 22 39.59	...	...	...	...	...	...	...	...	1.66	17.16	...
300.....	...	661	5 35 20.758	−5 21 55.34	M0(H)	...	M0	3850	0.49	1.6	1.57	13.48	1.27	10.79	...
301.....	...	...	5 35 20.775	−5 22 36.35	...	...	...	...	...	...	...	...	>2.7	17.54	...
302.....	...	9271	5 35 20.900	−5 23 21.93	M0(H)	...	M0	3850	0.72	0.39	3.65	15.75	1.21	12.53	...
303.....	...	...	5 35 20.986	−5 21 52.48	...	...	...	...	...	...	...	...	1.09	16.77	...
304.....	...	...	5 35 20.999	−5 22 54.45	...	...	...	...	...	...	...	...	1.70	16.04	...
305.....	...	9274	5 35 21.001	−5 22 23.01	M3:(H)	...	M2–M4	3350	0.77	0.16	4.99	17.02	1.45	13.36	...
306.....	...	9272	5 35 21.006	−5 23 55.87	...	...	...	...	...	...	5.07	15.95	1.29	12.78	...
307.....	...	9275	5 35 21.022	−5 22 25.49	cont + emis(H)	...	...	...	...	...	4.37	17.22	1.57	12.37	...
308.....	...	669	5 35 21.03	−5 23 49.05	G8(H) ≤ K5(P)K3(CK)K1–K2(Sam)	...	G8–K2	5250	0.37	13	1.67	10.76	...	...	...
309.....	...	...	5 35 21.108	−5 22 50.36	...	...	...	...	...	...	...	...	1.82	17.22	...
310.....	...	9277	5 35 21.166	−5 23 33.28	M6(H)	...	M6	2840	0.23	0.13	4.48	16.09	1.06	13.06	...
311.....	...	9276	5 35 21.183	−5 24 00.28	...	...	...	...	...	...	4.23	16.59	1.17	13.31	...
312.....	...	9278	5 35 21.211	−5 22 00.43	...	...	...	...	...	...	3.70	15.89	1.95	11.56	...
313.....	...	9280	5 35 21.237	−5 22 59.70	M3(H)	...	M3	3350	0.74	0.68	3.72	15.32	1.54	11.74	...
314.....	...	...	5 35 21.239	−5 23 16.95	...	...	...	...	...	...	...	...	2.47	14.20	...
315.....	...	...	5 35 21.268	−5 22 09.29	...	...	...	...	...	...	...	...	>2.2	17.70	...
316.....	...	9283	5 35 21.285	−5 22 15.86	M1.5(H)	...	M1.5	3595	0.82	0.20	...	16.83	1.31	13.28	...
317.....	...	681b	5 35 21.295	−5 23 46.18	...	...	...	...	...	...	3.99	16.39	1.38	12.85	...
318.....	...	679	5 35 21.312	−5 24 11.60	M0.5(H)K7:(P)	...	M0.5	3765	0.46	0.58	2.38	14.48	1.20	11.81	...
319.....	...	681a	5 35 21.357	−5 23 45.55	K7(P)	...	K7	4060	0.65	1.6	2.40	13.86	1.25	11.02	...
320.....	...	...	5 35 21.370	−5 22 07.60	...	...	...	...	...	...	...	...	2.29	13.70	...

NOTE.—Units of right ascension are hours, minutes, and seconds, and units of declination are degrees, arcminutes, and arcseconds.

[a] Designations of McCaughrean & Stauffer 1994.

[b] Designations of Hillenbrand 1997.

[c] Trumpler 1931 (T), Parenago 1954 (Par), Johnson 1965 (J), Strand 1958 (S), Levato & Abt 1976 or Abt & Levato 1977 (LA), Cohen & Kuhi 1979 (CK), Herbig & Terndrup 1986 and reference therein (HT), C. F. Prosser & J. R. Stauffer 1993, private communication (P), van Altena et al. 1988 (vA), Edwards et al. 1993 (Eetal), Samuel 1993 (Sam), Hamilton 1994 (Ham), Hillenbrand 1997 (H), and L. A. Hillenbrand 2000, private communication (Hp).

[d] The spectral type, K-band continuum veiling, and CO band head strength measured from the K-band spectra. The veiling at K is defined as $r_K = I_{2.2}$(IR excess)/$I_{2.2}$(star), which is estimated from the spectra. The strength of the CO band head is given as a percentage increase in CO absorption over that of a dwarf of the same spectral type.

[e] Blank entries indicate sources that are saturated or are too close to bright stars to be measured. The one exception is TCC003, which is not detected in the NICMOS data.

[f] McCaughrean & Stauffer 1994.

[g] Member of a binary system that is resolved in the optical measurements while unresolved in the IR photometry.

[h] The spectral type assigned to source 97 applies to the composite system of 97, 100, and 101.

[i] Within a diffraction spike.

[j] Hillenbrand 1997.

[k] Optical measurement listed for TCC046 probably includes both TCC039 and TCC046.

[l] Optical measurement listed for TCC073 includes both TCC070 and TCC073.

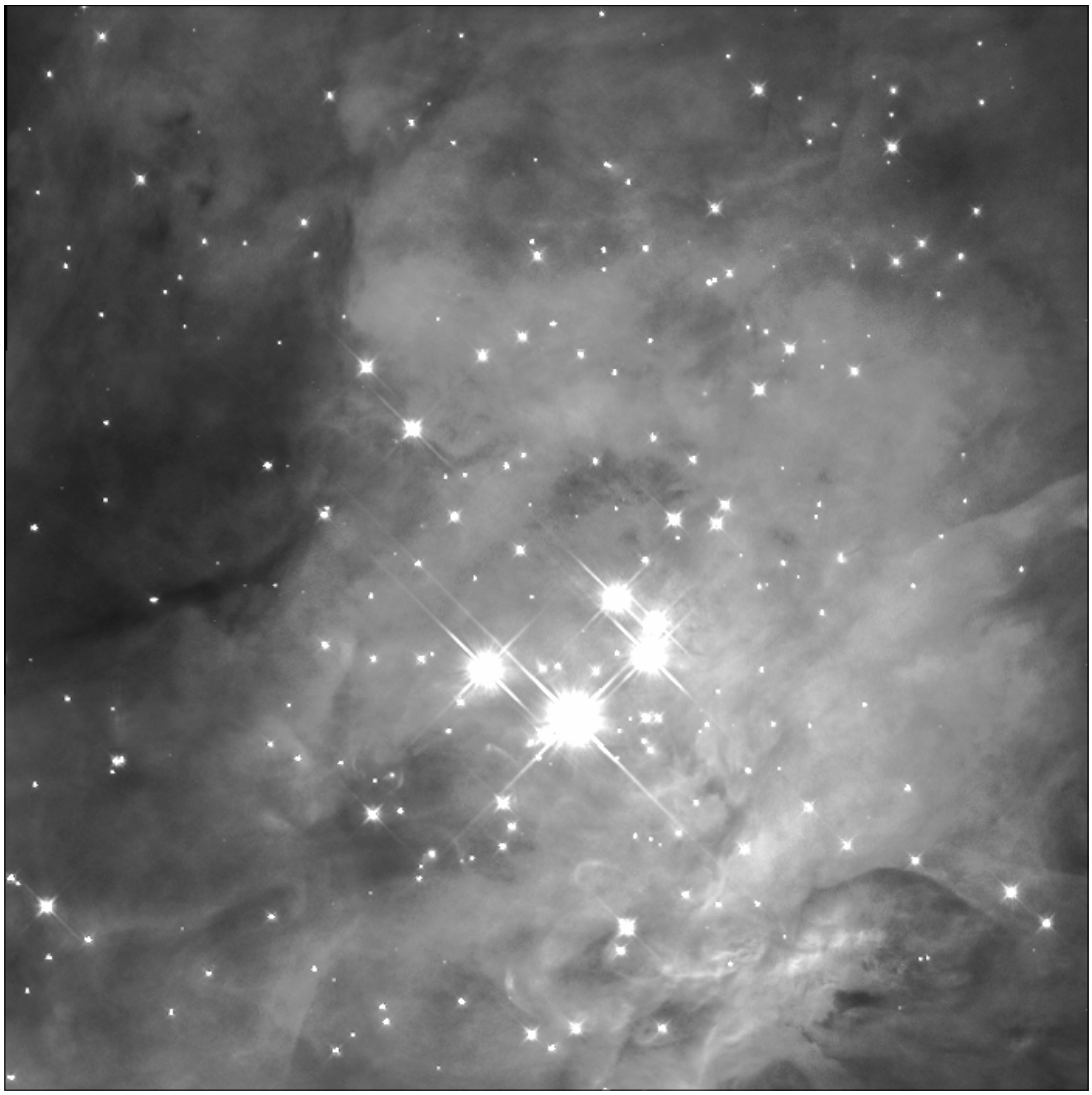

FIG. 1.—NICMOS F110W image of the Trapezium Cluster (140″ × 140″). The display range is from 0 to 0.3 mJy pixel^{-1}. East is left and north is up.

Stellar coordinates and photometry were measured from the NICMOS images with the package APPHOT within the IRAF environment. Initial identifications of sources with DAOFIND were checked through visual inspection. Given the high spatial resolution of the data, knots of nebulosity were easily rejected. A few sources accepted as stars have slightly extended profiles (45, 103, 215 in Table 1), possibly due to circumstellar material. Because the point-spread function (PSF) of *HST* is undersampled by NIC3, it can be difficult to distinguish a faint star from a cosmic-ray hit. However, nearly all objects that were identified by DAOFIND and through visual inspection were detected in at least two bands in the NICMOS and ground-based photometry (including unpublished *K*-band measurements of M. McCaughrean). An exception is source 65, which was quite faint and detected only in F160W. Several faint *K*-band sources of MS could not be measured with NICMOS owing to their close proximity to the OB stars.

Aperture photometry was extracted for all sources with the task PHOT using a radius of two pixels. The background level was measured in an annulus around each source and subtracted from the photometry. Because of the structure of the nebulosity, the background was measured as close as possible to each star by using an annulus one pixel wide. The inner radii of these annuli ranged from three to six pixels, where the larger annuli were required to sample the background emission properly around brighter stars.

The data were calibrated assuming 2.873×10^{-6} and 2.776×10^{-6} Jy ADU^{-1} s^{-1} and zero-magnitude fluxes of 1775 and 1083 Jy on the Vega system respectively for F110W and F160W. To apply this calibration, it is necessary to correct our small-aperture photometry to total signal. From bright stars in our images, we measured the aperture corrections from a radius of 2 to a radius of 7.5 pixels to be 0.125 and 0.150 mag for F110W and F160W, respectively. Additional corrections from 7.5 to 22.5 pixels were estimated from simulations of the PSF to be 0.030 and 0.046 mag for F110W and F160W. Stars brighter than $m_{110} \sim 10$ and $m_{160} \sim 9$ are saturated. Because of the variations in the nebulosity, the detection limits are not constant across the field, but are typically $m_{110} \sim 18$ and $m_{160} \sim 17$.

Except at these faintest limits, the photometric uncertainties are dominated by the undersampling of the *HST* PSF by the NIC3 detector. Because of the overlap among the images in the 3 × 3 grid of pointings, we have more than

FIG. 2.—NICMOS F160W image of the Trapezium Cluster (140″ × 140″). The display range is from 0 to 0.3 mJy pixel^{-1}. East is left and north is up.

one measurement for a large number of objects. The differences in the separate measurements were 0.2 mag or less for most sources; hence an approximate error in the photometry is no more than ± 0.2 mag. The $m_{110} - m_{160}$ colors, on the other hand, showed a smaller scatter. The separate pointings of *HST* at F110W and F160W may have been precise enough to produce similar samplings of the PSF, resulting in relatively accurate colors. The average of the available measurements for a given star is taken as the final photometry listed in Table 1.

To derive coordinates for the NICMOS sources, we used the stars in the overlapping regions to compute offsets among the nine F160W frames and to place the stars on the same pixel coordinate system. A plate solution was measured with coordinates of nonsaturated sources detected in *K*-band images of the NICMOS field (M. McCaughrean 1996, private communication). For stars that are saturated in the NICMOS frames, we adopted the *K*-band coordinates. The *K*-band data of McCaughrean do not provide precise coordinates for sources 127, 153, 154, and 191 and these stars are too close to bright stars to be measured in the NICMOS frames. We used the offsets of these stars from their bright neighbors as provided by MS to place them on the coordinate system (the declinations are the same and the right ascensions are 0.013 s greater in the coordinate system of MS compared with that of McCaughrean).

Table 1 lists all known optical and near-IR point sources within the NICMOS field (140″ × 140″) towards the Trapezium. Several close pairs in the *HST* images of Prosser et al. (1994) are unresolved in the NICMOS and ground-based data. These pairs are treated as one object and in § B the luminosities and reddenings are calculated from the combined photometry for the system. There is one fairly bright object ($K = 14$) that was observed by MS but not detected in the NICMOS images. It is probably very red or a knot of nebulosity that was unresolved in the ground-based data. Faint companions in the NICMOS images that are not detected in the *K*-band images include objects 67, 70, 218, 255, and 303. Because TCC 075 and TCC 077 are only partially resolved in the NICMOS data, photometry was extracted from the combined system. The *K*-band measurements of MS for these two objects were combined to produce the value listed in Table 1. The star ID 459 from the compilation of Hillenbrand (1997) is reported to have

$I_C = 12.5$, but has no measurement at V and is not detected in any of the IR data. This object is probably a ghost in the images of Jones & Walker (1988). In the NICMOS images, TCC 009 is nebulous and does not appear to be stellar. ID 459 and TCC 009 are excluded from Table 1.

2.2. *Individual Source Characteristics*

2.2.1. *A New CO Emission Source*

We have detected second overtone CO emission towards object 50, otherwise known as source n (Lonsdale et al. 1982). Spectra for this source and the BN object are shown in Figure 3. An H-band spectrum of source n is featureless at a signal-to-noise of 25. Source n and the BN object are the reddest objects with detections at both NICMOS bands, with colors of $m_{110} - m_{160} = 4.25$ and 5.44, respectively. Given the fairly high luminosity for source n implied by its K magnitude and very red colors, the CO emission probably arises from an inversion layer in an irradiated disk around a luminous, hot central star (Calvet et al. 1991; Biscaya Holzbach et al. 1999). Source n had received little attention until Menten & Reid (1995) observed a double radio source centered on it. Since CO emission usually is accompanied by outflows, our observations agree with and complement their proposal that source n drives a maser outflow and could contribute significantly to the energetics of this part of the BN/KL nebula.

2.2.2. *Spectral Types and Extinctions*

We determined spectral types for the Trapezium Cluster in a manner similar to our previous studies of other clusters (Luhman & Rieke 1998, hereafter LR98, LRLL, and LR99); therefore, we have placed the detailed description of this process in Appendix A. For similar reasons, we have used the same Appendix B for a discussion of the extinction determination and correction. We define the Trapezium spectroscopic sample as all objects in Table 1 that have spectral types, either IR types from this work and/or previously published optical types.

2.2.3. *Surface Gravities*

Because the ratio of Na and Ca to the CO band heads changes significantly with luminosity class (Kleinmann & Hall 1986), K-band spectra can be used to examine qualitatively the surface gravities of young stars. In previous studies by Greene & Meyer (1995) and Greene & Lada (1997), the relative strengths of the atomic lines and the CO band heads in young stars have appeared intermediate between the values for dwarfs and giants. This effect is largely due to the deepening of CO with lower surface gravity at a given spectral class, although the simultaneous weakening of Na in mid-to-late M stars is also a significant contributor (LRLL).

In Figure 4, the first band head of CO is plotted versus the sum of Na and Ca for the Trapezium, the $5' \times 5'$ core of IC 348 (LRLL), and the cloud core of ρ Oph (LR99). The solid lines represent fits to the measured equivalent widths of standard dwarfs and giants in LR98. The dwarf locus is shown for spectral types of M4V and earlier. At later types, the CO continues to strengthen while the atomic lines weaken (see LR98). The late M stars in the IR spectroscopic sample are faint and have low signal-to-noise data; hence the weak atomic lines cannot be measured accurately and we omit objects later than M4 in this analysis. As illustrated in Figure 4, the K-band spectra indicate lower average surface gravities from IC 348 to ρ Oph to the Trapezium, with a larger spread in gravities in IC 348. Since surface gravities should be lowest at the earliest stages of stellar evolution, we compare these results to the distributions of ages of these clusters implied by the DM97 evolutionary models in § 2.3.3. IC 348 is clearly older than the Trapezium and ρ Oph from both the inferred ages and the surface gravity diagnostics. The IR spectroscopic sample for the Trapezium in Figure 4 has the same distribution of ages as the entire spectroscopic sample (optical + IR) discussed in § 2.3.3. This distribution is younger than that in the ρ Oph cloud core, in agreement with the slightly lower surface gravities suggested for the Trapezium in Figure 4. However, when we account for selection biases in § 2.3.3, we find that the Trapezium and the cloud core of ρ Oph have similar ages.

2.2.4. *Effective Temperatures and Bolometric Luminosities*

Reddenings, effective temperatures, and luminosities for the six OB stars in Table 1 are taken from Hillenbrand (1997). For the remainder of the sample, we used the reddening corrections discussed in Appendix B and the spectral classifications and photometry to estimate temperatures and luminosities.

Spectral types of M0 and earlier are converted to effective temperatures with the dwarf temperature scale of Schmidt-Kaler (1982). LR98 considered the various M dwarf temperature scales and concluded that the conversion of Leggett et al. (1996) agreed with the data on the two eclipsing binaries, CM Dra and YY Gem. Luhman (1999) recently used the components of the young quadruple system GG Tau (White et al. 1999) and the locus of stars in IC 348 as empirical isochrones to test combinations of theoretical evolutionary models and temperature scales for very young objects. Although there is some discrepancy near the hydrogen burning limit, the dwarf temperature scale was compatible with the models of DM97 at higher and lower masses. Therefore, we will use the dwarf scale when our data are interpreted with the DM97 models, just as in our studies of IC 348 and ρ Oph. As a result, we will be able to compare the IMFs confidently among these clusters. The temperatures listed in Table 1 correspond to the average of the adopted spectral type ranges under the dwarf scale. The temperature scale that produces agreement between the model isochrones of B98 and the data for IC 348 and GG Tau is intermediate between the scales for M dwarfs and giants (see Fig. 7 of Luhman 1999). Therefore, we will use this temperature scale when calculating the IMF with the models of B98 in § 2.3.4.

The photometric bands R through H are the least susceptible to contamination from short or long wavelength excess emission (e.g., Meyer, Calvet, & Hillenbrand 1997). For the Trapezium data, the bolometric luminosities are measured from m_{160} except for a few cases discussed in Appendix B where m_{160} was not available and we used I_C. With the models of Allard, Alexander, & Hauschildt (1998), we estimate $m_{160} - H = 0.1$, 0.04, and 0.02 at effective temperatures of 3000, 4000, and 6000 K. A color of $m_{160} - H = 0.05$ is adequate for converting all BC_H to BC_{160}, where the dwarf bolometric corrections are the ones used by Luhman (1999). We arrive at the bolometric luminosities in Table 1 by combining the bolometric corrections, dereddened m_{160} or I_C, and a distance modulus of 8.27

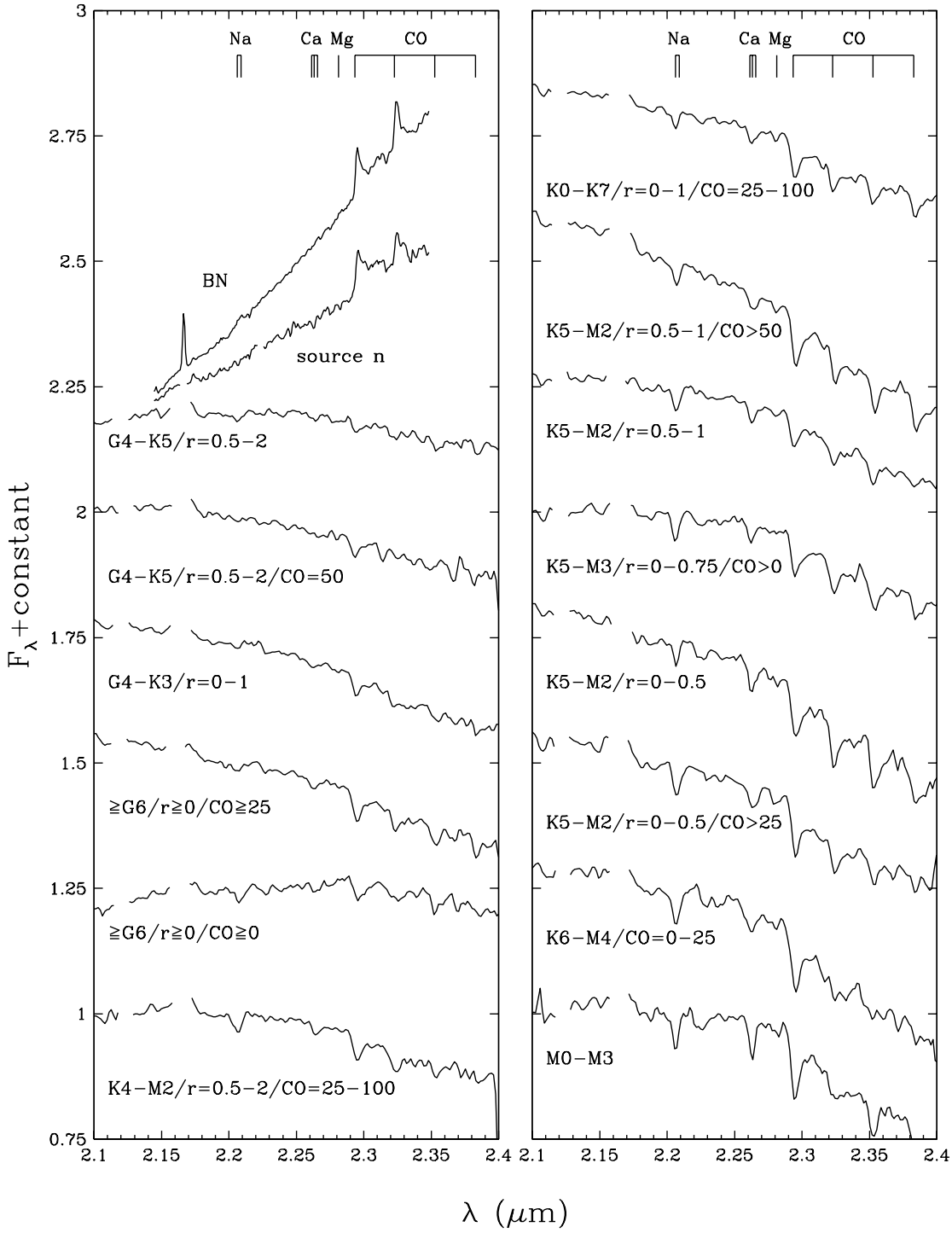

FIG. 3.—Composite K-band spectra of sources in the Trapezium Cluster. The spectra of BN and source n have $R = 1200$ and are normalized at 2.29 μm, while the remaining data have $R = 800$ and are normalized at 2.2 μm.

(Genzel & Stutzki 1989). The typical uncertainties in the luminosities are ± 0.15–0.2 dex in log $L_{\rm bol}$. These rather large errors are a result of reddening uncertainties due to variability between the observations at I_C and m_{160}, and to the undersampling of the NICMOS PSF, which affects all our NICMOS photometry.

2.3. *The Trapezium Stellar Population*

2.3.1. *Cluster Membership*

Given the very small area of sky covered by the Trapezium Cluster and the distance of Orion out of the Galactic plane, we expect very little contamination from field stars in the foreground. Stars 125 and 129 were rejected as nonmembers by Hillenbrand (1997) because proper motions were detected. The colors of these stars are redder than expected for foreground stars and one object appears to have enhanced CO absorption, supporting a pre–main-sequence nature. Nevertheless, we omit these stars from the remainder of our analysis. The $C^{18}O$ maps of Goldsmith, Bergin, & Lis (1997) indicate a large amount of extinction throughout the NICMOS field, with a gradient from east ($A_V \sim 30$) to west ($A_V \sim 100$). Because of this heavily

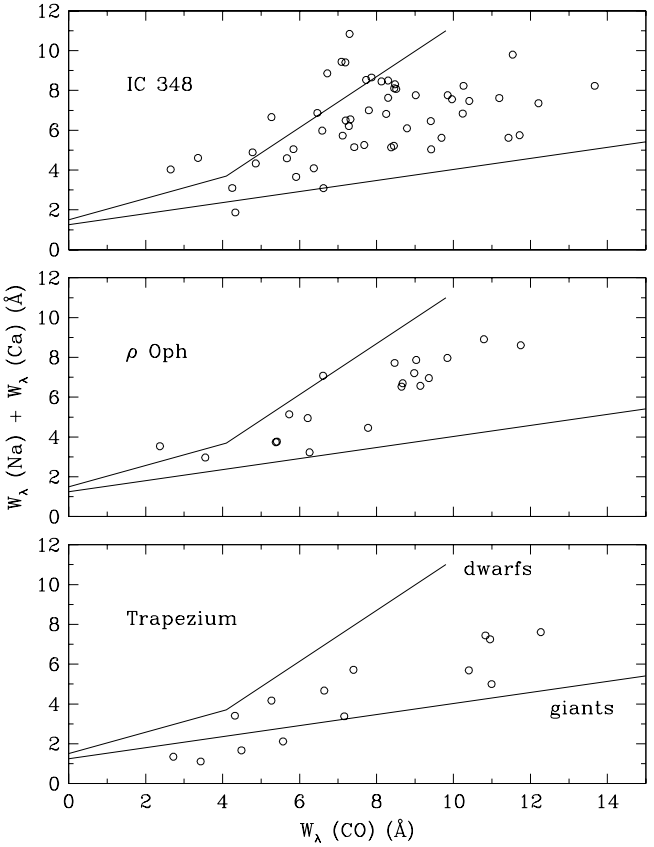

FIG. 4.—Equivalent widths of CO(2, 0) vs. the sums of the widths of Na and Ca in K-band spectra of young stars in the core of IC 348 ($5' \times 5'$; LRLL), the cloud core of ρ Oph (LR99), and the Trapezium Cluster. The equivalent widths for the Trapezium stars are measured from the composite spectra in Figure 3. The solid lines represent standard dwarfs (< M5V) and giants (< M0III) (LR98). Significant K-band continuum veiling can occur in very young stars, which dilutes the equivalent widths and moves the stars towards the origin. Typical measurement errors in the equivalent widths are 0.3–1 Å.

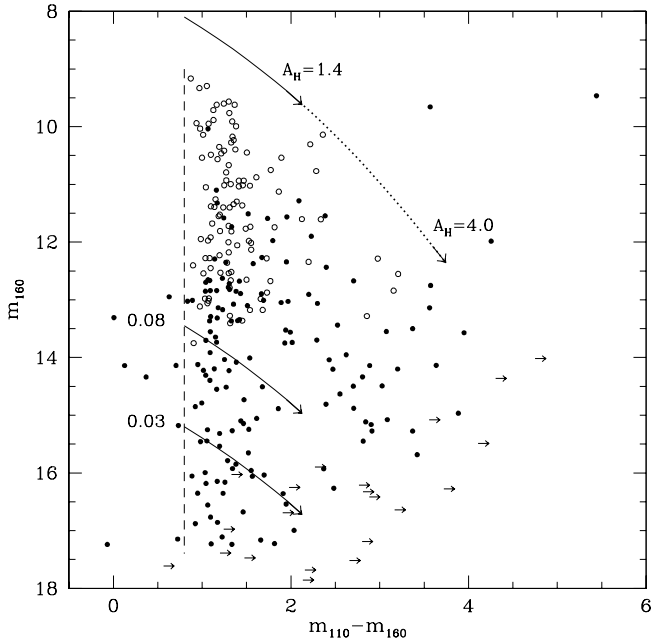

FIG. 5.—$m_{110}-m_{160}$ vs. m_{160} for the Trapezium Cluster (140″ × 140″). Stars with spectral types are represented by the open circles. The average intrinsic color (*dashed line*) is largely independent of spectral type for K and M stars. The upper curve represents the reddening vector in the NICMOS bands. Reddening vectors from A_H = 0-1.4 are also shown for 0.08 and 0.03 $M_\odot$ at an age of 0.4 Myr (D'Antona & Mazzitelli 1997). The IMF is constructed from sources with $A_H \leq 1.4$.

obscuring molecular cloud behind the Trapezium, no background stars should appear except at very large reddenings. We exclude background stars by including in our sample only stars with reddenings of $A_H \leq 1.4$, equivalent to $A_V \leq 8$. As seen in Figure 5, the distribution of colors remains constant as a function of magnitude within the low reddening sample, implying that the fainter sources are indeed an extension of the Trapezium population to substellar masses and not a contaminating population of heavily reddened background stars. The unique viewing geometry of the Trapezium Cluster has allowed us to detect this rather large population of brown dwarfs and thus measure the IMF to very low masses.

2.3.2. *The H-R Diagram*

To allow comparison of the Trapezium IMF to the previous measurements for IC 348 and ρ Oph, we first use the models of DM97 to infer masses from the source temperatures and luminosities. We then use the models of B98 to obtain the most accurate possible mass estimates to constrain the true form of the Trapezium IMF. B98 advise caution in the use of their models for very young clusters because they use atmospheres limited to surface gravities of $\log g \geq 3.5$, which corresponds to ages of $\gtrsim 1$ Myr. Nevertheless, as discussed by Luhman (1999) and White et al. (1999), the B98 models produce better agreement than any others with the few dynamical mass estimates for young stars and thus we adopt them as the most accurate available.

Because the B98 models do not include stars above 1 $M_\odot$, the B98 IMF is constructed in a somewhat different fashion than with DM97. As shown in Figure 6, the mass tracks of DM97 and B98 differ significantly for very young stars near 1 $M_\odot$. However, at higher masses and warmer temperatures, uncertainties in the treatment of convection are less important and the various models (e.g., DM97; Bernasconi 1996; F. J. Swenson 1996, private communication) agree fairly well at 2–3 $M_\odot$. Thus, for the B98 IMF we use the models of DM97 to infer masses at ≥ 2 $M_\odot$. To include the stars that fall above the 1 $M_\odot$ track of B98 and below the 2 $M_\odot$ track of DM97, we place these objects in one mass bin extending from $\log M = -0.05$ to 0.35 (0.89–2.2 $M_\odot$). This bin size is then used for the remainder of the B98 IMF as well, with a division by 2 to produce the same normalization as in the DM97 IMF.

The temperatures corresponding to the average of the adopted spectral type ranges and the luminosities for the Trapezium spectroscopic sample are plotted with the evolutionary models in the H-R diagrams in Figure 6. As discussed in § 2.2.4, for the M stars different temperature scales are used with the tracks of DM97 and B98. The highly reddened stars in Figure 6 are generally the youngest, particularly the ones embedded near the BN object.

Because of the large uncertainties in spectral types for some sources, for each star in the Trapezium sample we assigned 10 spectral types evenly spaced across the adopted range of types and calculated the resulting luminosities and reddenings. The spectral type uncertainties probably do not follow a Gaussian function, thus we simply assume a

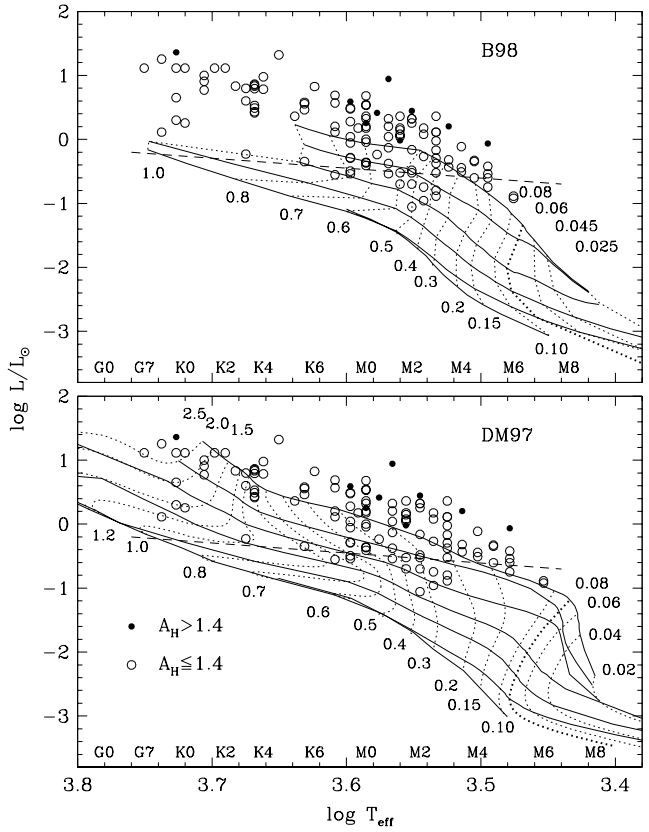

FIG. 6.—H-R diagram for the Trapezium Cluster (140″ × 140″). The theoretical evolutionary models of B98 (*upper*) and DM97 (*lower*) are shown, where the horizontal solid lines are isochrones representing ages of 0.3 (not available for B98), 1, 3, 10, 30, and 100 Myr and the main sequence, from top to bottom. The dashed line in the H-R diagram represents a dereddened magnitude of $K = 12$, above which the spectroscopic sample is representative for $A_H \leq 1.4$ (see Fig. 5). The M spectral types have been converted to effective temperatures with temperature scales that are compatible with each set of evolutionary models (Luhman 1999); a dwarf scale for DM97 and a scale intermediate between dwarf and giants for B98.

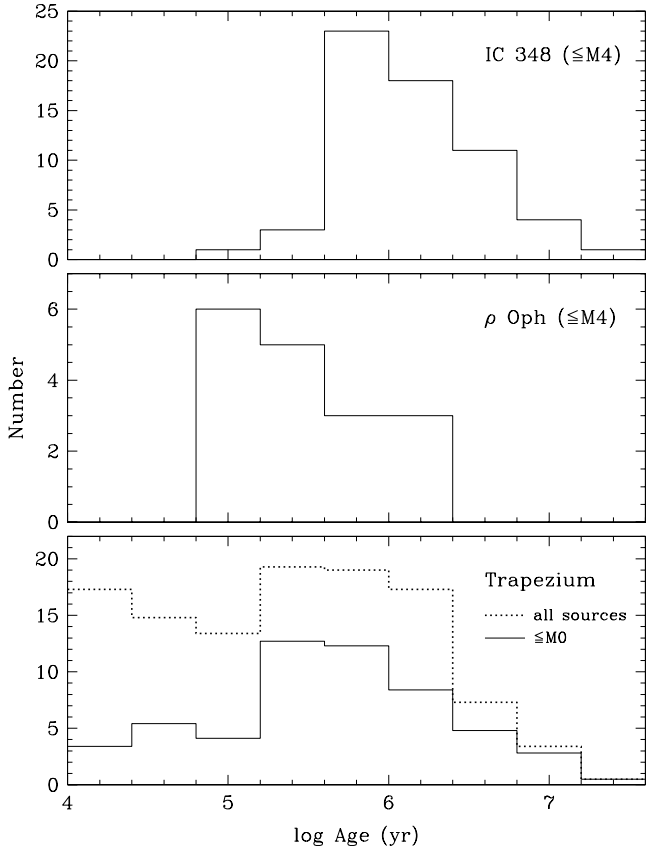

FIG. 7.—Distributions of ages inferred from the evolutionary models of DM97 for the core of IC 348 (5′ × 5′; LRLL), the cloud core of ρ Oph (LR99), and the Trapezium Cluster (140″ × 140″). Objects with spectral types later than M4 in IC 348 and ρ Oph have been omitted because the models of DM97 imply older ages for sources near the hydrogen burning limit. For the Trapezium, the distributions of ages for the entire spectroscopic sample (*dotted line*) and for stars M0 and earlier (*solid line*) are shown, where the latter should be representative of the stellar population.

uniform distribution. Each of the 10 masses and ages inferred for a star is given a weighting of 0.1 and added to the IMF and the distribution of ages.

2.3.3. *The Distribution of Ages*

The distribution of ages implied by DM97 for the Trapezium ($A_H \leq 1.4$) is shown in Figure 7. Although the youngest isochrone shown in Figure 6 is for 0.3 Myr, most of the tracks of DM97 do include ages close to 0.01 Myr. The few stars falling above this isochrone were placed in the youngest age bin. The OB stars have been excluded in Figure 7. The spectroscopic sample in the Trapezium is complete only for types earlier than M1 with a bias toward young objects for later types. We have omitted Trapezium sources later than M0 to derive a distribution that is representative of the cluster.

Although the absolute ages implied by evolutionary models must be interpreted with caution at such early stages, it is instructive to compare the distributions of ages from cluster to cluster. The models can indicate different ages as a function of mass in the same cluster, hence we must consider similar ranges of spectral types among the populations. Because the DM97 models produce systematically older ages near the hydrogen burning limit compared to higher and lower masses (Luhman 1999), objects later than M4 in IC 348 and ρ Oph are omitted (the spectroscopic samples in these regions are complete to M5). As illustrated in Figure 7, the ρ Oph cloud core and the Trapezium interpreted with DM97 have similar median ages (∼0.4 Myr). The 5′ × 5′ core of IC 348 has an older median age (1–2 Myr) and lacks the extremely young ages (<0.5 Myr) found in the other two clusters.

For all three clusters, our data are consistent with very short durations for the star formation. The true range of ages may be more narrow still because most forms of observational error will artificially broaden the age distributions. For example, because the evolutionary tracks are vertical on the H-R diagram at low masses for ages ∼1 Myr or greater, the ages of unresolved binary systems inferred from the H-R diagram will be younger than would have been deduced for the individual components. Thus, a coeval population with a mixture of binary and single stars will appear to have a significant range of ages.

2.3.4. *The IMF*

The Spectroscopic Sample.—The first step in constructing the Trapezium IMF was to assemble a sample observed spectroscopically, within the 140″ × 140″ NICMOS field towards the Trapezium, and with $A_H \leq 1.4$, which includes a majority of the Trapezium population while remaining

free of background stars (see § 2.3.1). Each binary system that is resolved in the *HST* data of Prosser et al. (1994) but not in the NICMOS images is treated as a single star. The partially resolved pair TCC 075 and TCC 077 is also treated as one star. The unresolved G-type companion to the B star 119 is ignored. All remaining sources have separations greater than 0.″7, a physical scale that is comparable to those resolved in ground-based studies (1″–2″) of IC 348 and ρ Oph. The resulting IMFs should be similar to the primary star mass functions, with the exception of binary companions at large separations, which will be included in the IMF under the above prescription.

For the six OB stars, we adopt the masses from Hillenbrand (1997). In studies of the Orion Nebula Cluster, Hillenbrand (1997) and Hillenbrand & Hartmann (1998) found evidence for mass segregation for stars above 5 $M_\odot$. They suggest that the concentration of the massive stars in the center of the cluster is likely primordial rather than due to dynamical effects. We do not account for this segregation in the IMFs shown in this paper. In such a correction, the four stars above 5 $M_\odot$ would be normalized to the number of stars in a reddening limited sample from the entire Orion cluster, which would reduce the counts in the most massive bins of the IMF by an order of magnitude.

The DM97 and B98 IMFs for the Trapezium spectroscopic sample are shown as the dashed histogram in Figures 8 and 9.

Sources Without Spectra.—In a similar manner as LR98, LRLL, and LR99, we estimate masses for the faint sources that lack spectra and are likely members and add them to the IMF. As previously discussed, we expect all objects within the reddening limit of the IMF calculation to be cluster members. This correction to the spectroscopic sample will be well-defined in terms of mass and extinction because (1) our photometry encompasses the wavelengths where cool, low-mass objects are luminous, (2) the NICMOS color is insensitive to intrinsic spectral types, (3) the IR photometry reaches reddened objects easily, (4) the directions of increasing reddening and decreasing mass are nearly perpendicular in an IR color-magnitude diagram (unlike in the optical), and (5) the abrupt increase in extinction between the Trapezium population and the background stars behind the molecular cloud assures us that there is no field star contamination in a reddening limited sample (see § 2.3.1). For this correction, we include all sources that lack spectral types, are detected at both m_{110} and m_{160}, and have $A_H \leq 1.4$. We omit the four sources with anomalously blue colors of $m_{110}-m_{160} < 0.5$. The unresolved binaries from Prosser et al. (1994) are treated as one star. For the sources with NICMOS photometry, reddenings are derived from $m_{110}-m_{160}$ as described in § B. In addition, there are a few sources that lack both spectral types and NICMOS photometry. Object 46 is not detected in the NICMOS images and hence is probably too red to be included in the IMF sample. Star 136 is saturated in the NICMOS data, but has I and K measurements that are similar to those of 113, 130, 187, and 238, which have inferred masses of 2–3 $M_\odot$. We therefore place 136 in the mass bin centered at log $M = 0.45$. Sources 120, 127, 153, 154, and 191 are too close to the OB stars to be measured by NICMOS and 145 falls within a diffraction spike. Because only K-band data are available for these six objects, we will adopt a reddening of $A_K = 0.3$, which is typical for the center of the Trapezium.

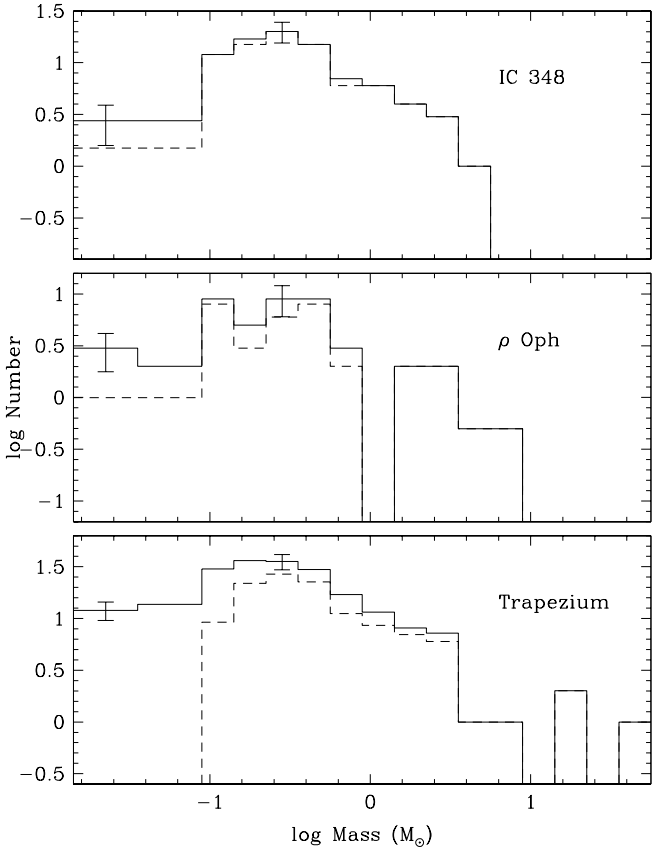

FIG. 8.—IMFs for the core of IC 348 (5′ × 5′; LRLL updated with data from Luhman 1999), the cloud core of ρ Oph (LR99), and the Trapezium Cluster (140″ × 140″) derived from the evolutionary models of DM97. The dashed histograms are measured from the spectroscopic samples in each region and the solid histograms include likely cluster members that lack spectral types. The two lowest mass bins are given widths of $\Delta\log M = 0.4$ because of the uncertainties in mass estimates. The IMFs are complete to log $M = -1.45$ and $\gtrsim$50% complete in the bin from log $M = -1.45$ to -1.85. To account for the segregation of the OB stars to the center of the Orion cluster, the values in the highest mass bins (>5 $M_\odot$) would be reduced by roughly an order of magnitude. The counting uncertainties are indicated by the error bars in the last bin and at the peak of the IMF.

By combining the dereddened photometry with the derived ages, we can estimate masses for the sources that lack spectra. We describe such a derivation of masses first with the DM97 models. The distribution of DM97 ages for Trapezium stars with spectral types earlier than M1 (omitting the OB stars) should be representative of the entire population (§ 2.3.3). We normalize this star formation history to the total number of objects later than M0—stars classified later than M0 or faint stars lacking spectral types. From this distribution, we subtract the histogram of ages for stars that fall in the spectroscopic sample that are later than M0; the resulting distribution should reflect the ages of the objects without spectral types (see Figure 10). For each such object, we estimate a mass by combining an age randomly drawn from the derived distribution with the dereddened m_{160} (or K) photometry, distance modulus, DM97 models, and bolometric corrections. After repeating this procedure 10 times for each source and computing the average of the 10 resulting masses, we arrive at masses that are added to the DM97 spectroscopic IMF, producing the final DM97 mass function in Figure 8. At times, the modeling produced masses falling below the lower limit of the plot

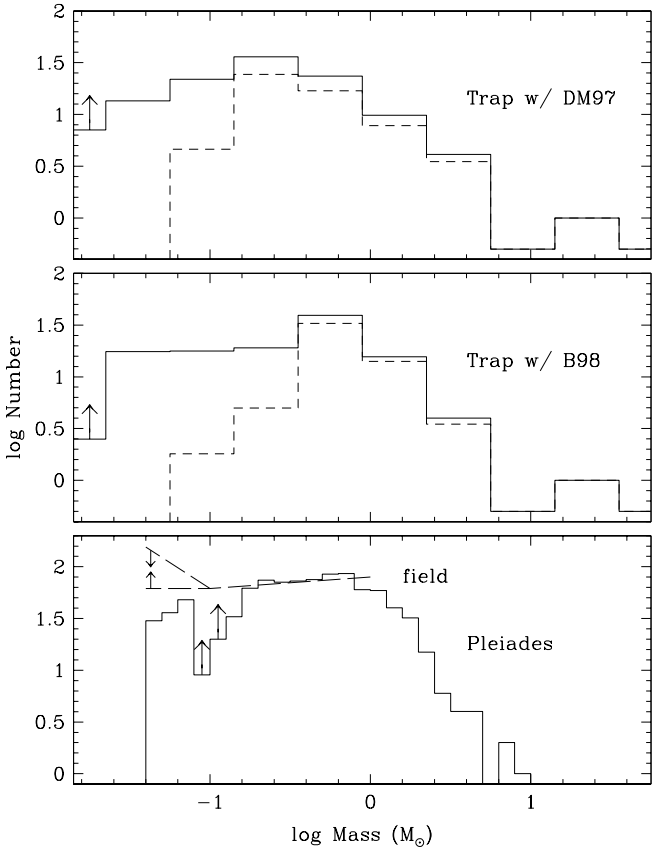

FIG. 9.—Trapezium IMFs inferred from the evolutionary models of DM97 (*upper panel*; same as Figure 8 but with larger bins) and B98 (*middle panel*). The B98 IMF is our best estimate of the true form of the IMF in the Trapezium, where the lowest mass bin is a lower limit because of incompleteness. The IMFs measured for the field (Reid et al. 1999) and the Pleiades (Bouvier et al. 1998) are given for comparison (*lower panel*). As indicated by the arrows and two dashed lines, Reid et al. (1999) constrained the substellar field mass function to have $0 \lesssim \alpha \lesssim 1$.

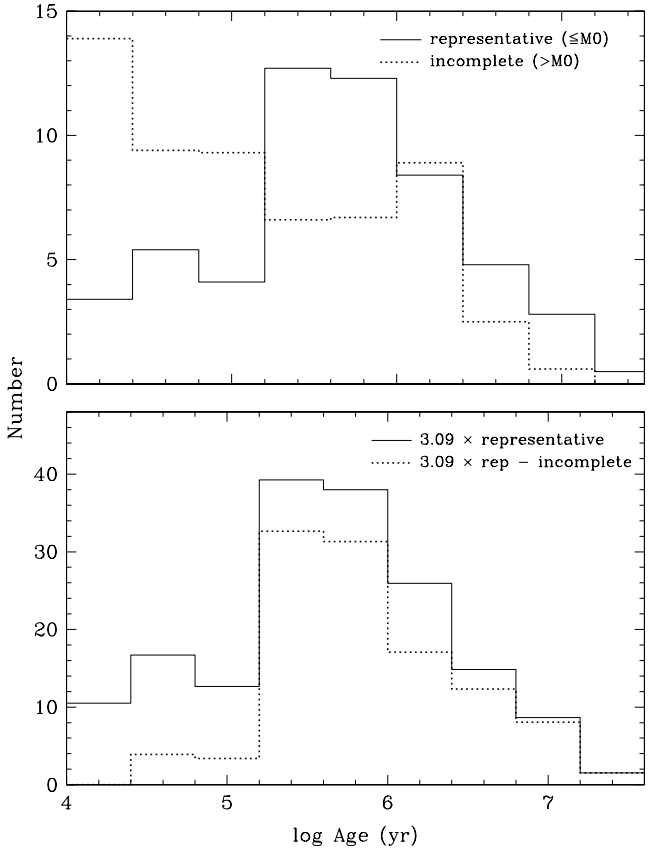

FIG. 10.—In the top panel, the distribution of DM97 ages for the Trapezium spectroscopic sample (Figure 7) is divided into earlier (*solid line*) and later type sources (*dotted line*). The sample with spectral types earlier than M0 should reflect the age distribution of the Trapezium, whereas the cooler objects are biased towards younger ages because of the spectroscopic completeness limit. In the lower panel, the early-type sample's representative distribution of ages is normalized (*solid line*) to the total number of objects that are likely to have types later than M0 (stars classified as later than M0 plus all objects with $A_H \leq 1.4$ lacking spectral types). This distribution minus the stars classified later than M0 produces a histogram of ages (*dotted line in lower panel*) that is used in estimating the masses of the objects lacking spectral types. These objects are added as a completeness correction to the IMF of the Trapezium in Figure 8.

of the IMF ($\log M = -1.85$). For instance, the faintest unreddened object in the color-magnitude diagram in Figure 5 is source 284 ($m_{160} = 17.1$, $m_{110} - m_{160} = 0.7$), which should have a mass of only $\sim 0.01\ M_\odot$ at the median age of 0.4 Myr for the Trapezium.

Because the evolutionary models of B98 do not include ages younger than 1 Myr, we cannot derive a distribution of B98 ages for the entire Trapezium Cluster, and thus we cannot estimate B98 masses for the sources lacking spectra in exactly the same manner as done with the DM97 models. Instead, we adopt one age for all sources lacking spectral types in estimating their B98 masses. The appropriate age is the median with these models of ~ 1 Myr, as indicated in Figure 6. This method should be equivalent to that used with DM97 for the following reasons. First, the mass bins that we have selected for the B98 IMF are so wide that the adopted age has little effect on the mass bin that an object falls in. We have also used the DM97 models to test how the mass function is affected by the adoption of a single age for all sources rather than a distribution of ages. We derived DM97 masses for the sources lacking spectra first by randomly drawing ages from the star formation history, as done in the previous paragraph, and then by adopting the median DM97 age of 0.4 Myr for all. We find that the resulting mass functions are the same within the counting uncertainties. Thus, we expect that adopting the median of 1 Myr in estimating the B98 masses should produce a mass function that is similar to the one we would find if we were able to apply a full distribution of ages. After accounting for these sources that lack spectra, we arrive at the final form of the B98 IMF in Figure 9; this mass function includes a population of ~ 50 likely brown dwarfs.

The above addition to the Trapezium IMF should be incomplete at the lowest masses because older or reddened brown dwarfs can fall below the detection limit of the NICMOS photometry. For instance, a brown dwarf at a mass of $0.02\ M_\odot$ and an age of 3 Myr would appear at the detection limit of $H = 17$. To estimate the completeness of the substellar IMF, we construct a population of brown dwarfs that is distributed uniformly across the mass bins from $\log M = -1.45$ to -1.65 and $\log M = -1.65$ to -1.85. For each mass, an age is randomly drawn from the distribution of ages that is representative of the Trapezium, as performed earlier in this section. An apparent H-band magnitude is inferred for each mass and age from the models of DM97. The combined distribution of magnitudes predicted for each mass bin is then compared to the limits of

the photometry. We find that the mass bins from $\log M = -1.45$ to -1.65 and $\log M = -1.65$ to -1.85 are $\sim$90% and $\sim$60% complete, respectively. We do not correct for this incompleteness in Figures 8 and 9 and instead wait for deeper photometry and spectroscopic confirmation of some of these brown dwarfs. However, this simulation suggests that the mass function in the Trapezium could be flat down to 0.01–0.02 $M_\odot$, as found for the somewhat older cluster σ Ori (Zapatero Osorio et al. 2000).

3. THE INITIAL MASS FUNCTION IN DIFFERENT ENVIRONMENTS

3.1. *Star-Forming Clusters*

Uncertainties in the theoretical evolutionary tracks can influence the shape of the IMF derived for young clusters. However, in comparing clusters with similar star formation histories, these effects will distort the derived IMFs in similar ways. That is, issues with the theoretical tracks will cancel to first order. Therefore, we use the DM97 tracks for comparisons among the three clusters we have studied in depth, IC 348, ρ Oph, and the Trapezium. Although we believe the B98 tracks are more accurate, those of DM97 have the advantages of extending to younger ages, and of providing the reader with a straightforward comparison with our previous work, which used the DM97 tracks.

3.1.1. *The IMFs in IC 348 and ρ Oph*

LRLL used a combination of spectroscopy and photometry to construct the IMF for members of the $5' \times 5'$ core of IC 348. Luhman (1999) obtained spectra of additional low-mass candidates for which only photometry had been available previously, identifying five new members and several background stars. To compute the IMF and examine the completeness, we consider sources from these two references and with $A_V < 7$, a sample that includes all but two of the known cluster members towards the core.

A recent proper motion study of IC 348 (Scholz et al. 1999) has provided membership probabilities for the foreground, background, and cluster populations within a square degree surrounding IC 348 at $R < 18$. These data are not definitive for distinguishing between cluster members and background stars. Many stars have high probabilities of belonging to both populations and several stars that are clearly cluster members by their photometry and spectra are given low cluster membership probabilities. Foreground stars are more confidently identified. Sources 77 and 121 from LRLL are probably in the foreground, which is consistent with the low reddenings implied by their colors and the lack of emission lines or IR excess. Both stars were considered cluster members by LRLL, and 77 was included in the IMF calculation of the cluster core. We omit 77 from the IMF shown here. The cluster memberships of the vast majority of the remaining sources in LRLL and Luhman (1999) are established by properties such as reddened colors and spectra, emission lines, IR excess emission, and gravity-sensitive spectral lines.

We took the masses of the cluster members observed spectroscopically from LRLL and Luhman (1999). To determine the IMF, we must add any likely cluster members that lack spectral types. Three objects from LRLL (96, 230, 248) appear to have late-type IR spectra (>K5), and therefore cannot be in the background because of their brightness. The reddening of these three stars is low, so they could be in the foreground. But because they were not identified as foreground stars in the proper motion study of Scholz et al. (1999) and because of the low probability of foreground star contamination towards the small area of the core (Herbig 1998), we take them to be cluster members for this analysis. IC 348 does not have a thick background molecular cloud; thus, background stars can appear in the photometry at low reddenings. However, member brown dwarfs have higher values of $R-I/J-H$ and $I-K/J-H$ than reddened field stars (see, e.g., Luhman 2000). By combining R and I photometry (Luhman 1999) with JHK data for the cluster core (LRLL), we identify and reject the background stars in the core down to very faint limits ($H \lesssim 16.5$) and identify five additional brown dwarf candidates listed in Table 2. Source 435 falls below the locus of cluster members in a diagram of $R-I$ versus I (Luhman 1999), but this is likely the result of blue excess emission, as suggested by the abundance of strong emission lines in its optical spectrum. Reddenings for these eight objects are measured from $J-H$ assuming an intrinsic color of 0.7. Masses are estimated by combining the dereddened H magnitudes with the DM97 models for an assumed age of 3 Myr. The resulting IMF is given in Figure 8.

The magnitude ($H \sim 16.5$) and reddening limits ($A_V <$ 7–8) are similar between the completeness corrections for the Trapezium and IC 348. Since the differences in distances and ages tend to cancel, we expect the substellar IMF in IC 348 to have a similar completeness level as described earlier for the Trapezium.

The mass function for ρ Oph is taken directly from LR99 and may still be slightly incomplete in the substellar range. For this cluster, the results from our analysis have been shown to be in excellent agreement with analyses based on photometry alone (e.g., Williams et al. 1995; Comerón, Rieke, & Rieke 1996). This agreement is improved if these earlier analyses are corrected approximately to expectations for the DM97 tracks (which would tend to reduce the portion of very low mass objects slightly). This agreement

TABLE 2

LOW-MASS CANDIDATES IN IC 348

ID	α(2000)	δ(2000)	$R-I$	I	$J-H$	$H-K_s$	K_s
435.....	3 44 30.33	32 11 33.9	1.45	18.95	1.20	0.85	14.24
603.....	3 44 33.43	32 10 29.8	...	19.93	1.01	0.65	15.17
609.....	3 44 44.92	32 09 34.7	...	21.20	0.99	0.36	16.89
618.....	3 44 43.92	32 08 34.3	...	21.47	0.94	0.47	16.89
624.....	3 44 26.30	32 08 08.7	...	21.83	1.01	0.67	16.43

NOTE.—Units of right ascension are hours, minutes, and seconds, and units of declination are degrees, arcminutes, and arcseconds. The optical and IR photometry is from the work of Luhman 1999 and Luhman et al. 1998, respectively.

supports our use of a combination of spectroscopic and photometric methods to arrive at complete IMFs, since there appear to be no significant systematic differences in the results of the two approaches.

3.1.2. *Comparison of IMFs in IC 348, ρ Oph, and the Trapezium*

It can be difficult to make meaningful comparisons of reported mass functions because of differing methodology and the wide range of environments investigated (Scalo 1998). For instance, the field star mass function of Reid & Gizis (1997) (updated by Reid et al. 1999) differs significantly from the mass functions determined in other studies (Kroupa 1995a, 1995b; Gould, Bahcall, & Flynn 1997). In Figure 11 the IMFs reported recently for the Pleiades (Bouvier et al. 1998) and the field (Reid et al. 1999) are similar, but these mass functions do not match that of Orion (Hillenbrand 1997). One would have expected the mass functions in the Pleiades and Orion to be similar, since they are both dense clusters and differ primarily in age.

At least some of these variations arise because different techniques (colors vs. spectral types) and evolutionary models (DM97 vs. B98) are often employed in converting data to masses. To illustrate, we compare our IMF for the center of the Trapezium ($D = 140''$) to the results reported by Hillenbrand (1997) for the larger Orion Nebula Cluster ($D = 18'$). The IMF of Hillenbrand is based on the DM94 tracks and has a small excess and a deficit of stars from 0.1–0.25 and 0.4–1 $M_\odot$, respectively, relative to our DM97 IMF shown in Figure 8. This difference persists when the comparison is restricted to stars in common between the two studies. However, when we adjust the luminosities estimated by Hillenbrand to the distance that we have adopted and derive masses for her data from the models of DM97 rather than DM94, the revised version of Hillenbrand's IMF agrees well with our measurements. While theoretical tracks for low-mass stars are mostly vertical on the H-R diagram for ages $\gtrsim 1$ Myr, they do exhibit significant dependence on both temperature and luminosity at younger stages, hence the dependence of mass on the estimated luminosity for the Trapezium. Unfortunately, the deficit of stars at 0.4–1 $M_\odot$ and the peak at 0.2 $M_\odot$ in the DM94 IMF of Hillenbrand have been referred to as real features of the IMF (Sirianni et al. 2000).

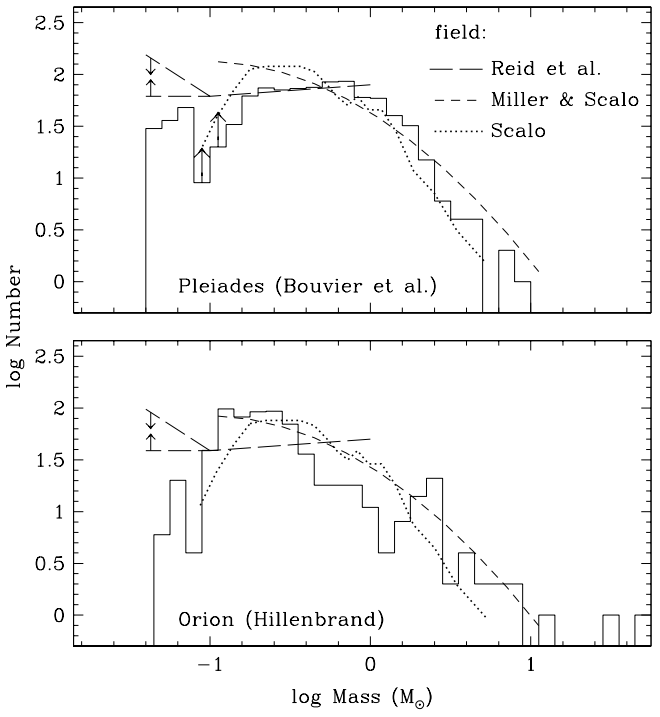

FIG. 11.—IMFs reported for the Pleiades and Orion by Bouvier et al. (1998) and Hillenbrand (1997) are compared to the recent field mass function (<8 pc) of Reid et al. (1999), where the slope of the field substellar mass function is constrained to be $0 \lesssim \alpha \lesssim 1$. The mass functions of Miller & Scalo (1979) and Scalo (1986) are also shown for reference.

Whereas the results of Hillenbrand (1997) used the models of DM94 and were complete to 0.1 $M_\odot$, the Orion IMF of Hillenbrand & Carpenter (2000) was based on the models of DM97 and reaches 0.02 $M_\odot$. After comparing the IMF of Hillenbrand & Carpenter (2000) (their Figure 16) to our DM97 IMF (Figure 8), we find that they are in agreement; they both show a peak near 0.2 $M_\odot$ followed by a slow decline and flattening into the brown dwarf regime.

Our studies of IC 348, ρ Oph, and the Trapezium cluster use homogeneous observational approaches and interpret the data with similar analyses using one theoretical foundation. The similarity in ages among these clusters causes most potential sources of systematic error to cancel to first order. Therefore, we can reliably search for variations in the low-mass IMF across 2 orders of magnitude in stellar density (ρ Oph, $n = 0.2$–1×10^3 pc^{-3}; IC 348, $n = 1 \times 10^3$ pc^{-3}; Trapezium, $n = 1$–5×10^4 pc^{-3}) and the accompanying range in star formation efficiency. As seen in Figure 8, the IMFs in IC 348, ρ Oph, and the Trapezium are quite similar. With the evolutionary models of DM97, the IMFs are characterized by a slow increase from substellar masses to ~ 0.25 $M_\odot$, and a drop with a slope of ~ 0.7 (Salpeter (1955) is 1.35) from 0.25 to 3 $M_\odot$. The mass functions from brown dwarfs to the lowest mass stars are similar between the Trapezium and ρ Oph. This comparison has the highest weight because of the very similar ages of the clusters. To first order, the IMF for IC 348 is also similar to those for the other two clusters. To second order, there appear to be proportionately fewer brown dwarfs in the core of IC 348. This tendency is only of modest statistical significance (compare the demonstration by Elmegreen 1999a of the effects of statistics on the high mass IMF). A better comparison of the substellar mass functions requires spectroscopy of the brown dwarf candidates that comprise the completeness corrections in these clusters to confirm their cluster membership and measure more precise masses. In addition, the spectroscopy survey begun by Luhman (1999) of all of IC 348 should eventually provide much better number statistics ($\times 3$) for comparison to ρ Oph and the Trapezium.

Above a few solar masses, the IMFs in the clusters IC 348, ρ Oph, and the Trapezium are the same within the uncertainties. Better number statistics can be achieved in richer, distant populations. For instance, in observations of clusters in the Large Magellanic Cloud, Hunter et al. (1997) and Massey & Hunter (1998) found that the IMF above 1 $M_\odot$ was invariant with cluster density over 2 orders of magnitude. Scalo (1998) found that the various IMFs reported in the literature for this mass range cannot be easily reconciled, even among studies of the same regions. If the variations in the mass function are real, they do not appear to depend on metallicity, stellar density, or Galactocentric radius (Scalo 1998). Elmegreen (1999a, 1999b) suggests that much of the variation in the measured slopes of

the IMF arises from statistical fluctuations and that there may be a common IMF at intermediate masses.

3.2. *Star-Forming Clusters, Young Open Clusters, and the Field*

While no set of theoretical evolutionary models agrees with observational tests at all ages, masses, and metallicities, White et al. (1999) and Luhman (1999) concluded that the models of B98 are the most consistent with the observational constraints available for very young low-mass stars. In addition, Luhman (1999) found that a temperature scale intermediate between those of M dwarfs and giants produced the best agreement between the B98 calculations and observations. By combining this temperature scale with the models of B98, we should arrive at the most accurate IMF currently possible for a young stellar population.

The DM97 and B98 IMFs for the Trapezium and mass functions of the Pleiades and the field are compared in Figure 9. With the DM97 models, the IMF in the Trapezium (and the other star-forming clusters) peaks near $\sim 0.25\ M_{\odot}$. In the more accurate B98 IMF, the peak shifts to higher masses and the shape is quite similar to the results in the Pleiades and the field; the differences between the previous Orion IMF and the other two regions shown in Figure 11 are now removed. In addition, Barrado y Navascúes et al. (2000) have recently reported that the stellar IMF for the M35 open cluster is similar to that of the Pleiades. We find that the data for the Trapezium, the Pleiades and M35 open clusters, and the field are all consistent with the same mass function, one that is flat or slowly rises from substellar masses, and rolls over between 0.6 and 1.0 $M_{\odot}$ into a falling power law toward high masses. The slope of the Trapezium B98 IMF from $\log M = -0.25$ to -1.45 (0.56–0.035 $M_{\odot}$) is ~ -0.3 (Salpeter is 1.35). As illustrated in Figure 9, because of the more pronounced peak in the Trapezium IMF compared to the Pleiades (which could be a second order systematic error from the methods and models), the computed slope for the Trapezium low-mass IMF is sensitive to the mass limits that are selected.

It is not surprising that the IMFs of the Trapezium and the Pleiades are similar since the Pleiades is a rich open cluster that was probably much like the Trapezium when it was younger. Furthermore, the similarity of these cluster IMFs to the mass function in the field is consistent with the suggestion that the field is predominantly populated by stars that formed in clusters (Lada, Strom, & Myers 1993). Since we might have expected a high degree of similarity among the mass functions, the observed agreement can alternately be taken as a demonstration that the methods for deriving the mass functions are consistent.

The data for the star-forming clusters and the young open clusters are most useful for studying the IMF when combined to complement each other. Because the stars in clusters like the Pleiades and M35 are free of excess emission and significant reddening, temperatures and luminosities are more accurately measured as compared to very young stars. In addition, because the open cluster members are near the main sequence, the theoretical models should be more robust and provide better mass estimates. These open clusters are also very rich and provide excellent number statistics, particularly in M35. Thus, the detailed structure of the IMF is more readily determined in regions like the Pleiades and M35. On the other hand, as noted by Bouvier et al. (1998), the IMF measured for the Pleiades may be a lower limit at low masses because of observational incompleteness and possible mass segregation. The substellar population is more luminous in clusters at the age of Orion and significant dynamical evolution has not occurred, allowing the measurement of the IMF down to much lower masses than possible in the open clusters. From the work presented here, we find no obvious decline in the density of sources down to the detection limit of 0.02 $M_{\odot}$ and probably, with a correction for incompleteness (§ 2.3.4), down to 0.01–0.02 $M_{\odot}$.

3.3. *Comparison with Other Studies*

The three young clusters in our study are by a significant margin the most thoroughly studied. However, the information available on other similar regions appears to be consistent with our results. Comerón, Rieke, & Rieke (1996) used photometric techniques to find a similar flat low-mass IMF to below the stellar limit in NGC 2024. Comerón, Rieke, & Neuhäuser (1999) showed that a flat IMF is also consistent with their data on Cham I. There are indications in a few older open clusters for a deficiency of low-mass members (e.g., Hawley, Tourtellot, & Reid 1999). However, for all of these clusters, there are concerns about the possible roles of dynamical evolution and mass segregation, about distinguishing members from background stars, and about the completeness of the known membership lists given the fading of the low-mass objects to or below the detection limits achieved in the near-IR and X-ray regions used for their identification. The available data for young open clusters are, in our view, all consistent with a common IMF of the form we have derived for the IC 348, ρ Oph, and the Trapezium.

We can also compare with recent estimates of the IMF in globular clusters and the bulge. Paresce & De Marchi (1999) concluded that the data on various globular clusters are consistent with a log-normal IMF with a characteristic mass of 0.33 $M_{\odot}$. Towards the Galactic bulge, Zoccali et al. (2000) report an IMF with a slope of 0.33 from 0.15–0.5 $M_{\odot}$ and one similar to that of Salpeter ($\alpha = 1.35$) from 0.5–1 $M_{\odot}$. These estimates, particularly the one for globular clusters, appear to differ significantly from the form of the IMF we find for young clusters and the field. This difference suggests that there may be a detectable variation in the IMF if the star-forming conditions are changed sufficiently. Although the conditions that prevailed for globular clusters are now impossible to determine observationally, this result should encourage searches for variations in other environments.

3.4. *Implications for Theories of the IMF*

Given the shape of the low-mass IMF that we have measured, its approximate invariance at stellar masses among local regions of clustered star formation, and the constraints on the minimum mass of free-floating objects, what are the implications for theories of the origin of the mass function?

Previous studies indicate that the IMF flattens below 1 $M_{\odot}$ (Scalo 2000). Our observations of IC 348, ρ Oph, and the Trapezium, with data for the Pleiades and M35 open clusters and the field, show that the effect occurs between 0.6 and 1 $M_{\odot}$, which can be interpreted in terms of a characteristic mass of the IMF. When the origin of the IMF is attributed to random sampling of the hierarchical structure of molecular clouds (Henrikson 1986, 1991; Larson 1992;

Elmegreen 1997, 1999a), the IMF should flatten or turn over near the Jeans mass. This parameter is not likely to vary significantly among nearby star-forming regions (Elmegreen 1999a), although such a conclusion could break down when the details involved in determining the Jeans mass are included (Myers 1998). Other theories (e.g., Silk 1995; Lejeune & Bastien 1986; Murray & Lin 1996) can produce a flattening of the IMF without any consideration of the Jeans criterion (Scalo 2000); for example, a turnover has been suggested to arise at or above the deuterium-burning mass (Shu, Adams, & Lizano 1987).

The Jeans mass is a function of the gas temperature and cloud-core pressure, and these properties in turn depend on Galactocentric distance. It is unclear if the characteristic mass we find in the IMF is indeed related to the Jeans mass without observing the low-mass IMF in clusters that span a wide range of Galactocentric distances. The lower characteristic mass in globular clusters is encouraging that such variations will be found if a sufficiently large range of conditions can be probed.

Scalo (1998) has already stressed that there is little evidence for a log-normal IMF. Data for globular clusters have been fit by a log-normal IMF (Paresce & De Marchi 1999), but because there are no constraints on the substellar mass functions in these regions, a true log-normal distribution cannot be verified. The IMFs in the Trapezium, the other young clusters, and the field are clearly not log-normal, contrary to the predictions of some models (Klessen, Burkert, & Bate 1998). Adams & Fatuzzo (1996) also derived a log-normal IMF in the case that a large number of independent variables determine the masses of stars. For a smaller number of such variables, a power-law tail appeared at high masses, which could match the form of the observed high-mass IMF. However, the IMF in the Trapezium and other clusters is approximately flat down to 0.01–0.02 $M_\odot$ and it is unclear whether the models of Adams & Fatuzzo (1996) can reproduce such a dramatic deviation from log-normal form.

The turnover in the IMF is fairly similar among clusters which include a large range of stellar densities and star formation efficiencies. This result is consistent with theories where the masses of stars are determined by processes of accretion and outflows (Adams & Fatuzzo 1996), instabilities related to stellar winds (Silk 1995), or hierarchical fragmentation (Elmegreen 1999a), but difficult to reconcile with suggestions that the stellar masses are controlled by dynamical interactions among stars and protostars (Price & Podsiadlowski 1995; Bonnell et al. 1997) or collision and coalescence of clumps (Lejeune & Bastien 1986; Murray & Lin 1996). In these latter cases, the properties of the IMF, such as the ratio of high to low-mass stars and the turnover mass, should depend on stellar density.

The shape of the substellar mass function and the minimum mass observed for free-floating objects are powerful constraints for theories of the IMF. We find that brown dwarfs can form in moderately large numbers, whereas a minimum mass of $\sim 0.1\ M_\odot$ is predicted by some models of hierarchical fragmentation (Larson 1992). Furthermore, it appears that free-floating objects can form at masses near ($\sim 0.015\ M_\odot$; Zapatero Osorio et al. 1999) and below ($\sim 0.01\ M_\odot$; this work and Zapatero Osorio et al. 2000) the deuterium burning limit (0.013–0.015 $M_\odot$; Burrows et al. 1997). This behavior is contrary to the expectations of wind-limited models (Shu et al. 1987). In fact, most theories of star formation have difficulty in explaining the abundance and minimum mass of brown dwarfs that we observe (see Elmegreen 1999b).

From millimeter-wave continuum observations in Serpens (Testi & Sargent 1998) and ρ Oph (Motte, André, & Neri 1998), it appears that the mass function of apparently prestellar clumps is reminiscent of the stellar mass function in the field. Umemoto et al. (2000) have identified clumps in ρ Oph using $H^{13}CO^+$ emission; the resulting clump mass spectrum is similar to that of Motte et al. (1998) but shifted toward higher masses by a factor of 3 to 4. The discrepancy may arise through modification of millimeter-wave emission properties of grains in dense clumps (Kruegel & Siebenmorgan 1995).

LR99 showed that the stellar IMF in ρ Oph determined with the DM97 tracks bears a close resemblance to the clump mass function in the same region determined by Motte et al. (1998). Use of the more accurate B98 tracks shifts the turnover mass in the stellar IMF upward. As shown in Figure 12, the turnover lies above that of the Motte et al. clump spectrum; it lies below the turnover in the Umemoto et al. spectrum. In both cases, the agreement is within a factor of 2. Given the potential errors in measuring the clump masses, it is possible that we are seeing evidence for a connection between the process of cloud fragmentation and the IMF. Better number statistics and mass accuracies and completeness to lower masses are required to confirm this possible relation. In particular, the

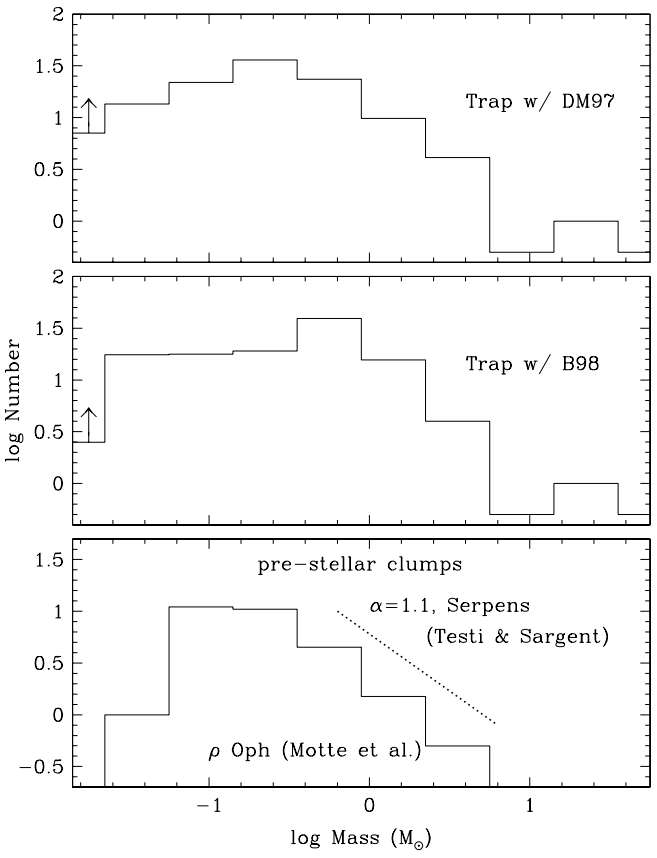

FIG. 12.—Trapezium IMFs inferred from the evolutionary models of DM97 and B98 are compared to the mass functions of prestellar clumps in Serpens (best-fit power law; Testi & Sargent 1998) and ρ Oph (*histogram*; Motte et al. 1998). The clump mass functions are incomplete below a few tenths of a solar mass.

clump mass function should be measured where the stellar IMF is most distinctive, below the turnover mass and into the brown dwarf regime.

4. CONCLUSION

The shape of the low-mass IMF ($<1\ M_\odot$) has remained uncertain because of several issues, the most important being incompleteness for faint low-mass stars and brown dwarfs. In observations summarized in this work, we have made reliable measurements of the IMF down to well below the hydrogen burning limit and have presented a robust comparison of the low-mass IMFs in local regions of clustered star formation. Our results are as follows:

1. Despite a range of 2 orders of magnitude in the density of star formation, the *stellar* IMFs in the core of IC 348 and the cloud core of ρ Oph are the same as in the Trapezium within the uncertainties. The IMFs in the *brown dwarf* regime are also roughly similar, although more observations are required for a definitive comparison of the substellar mass functions.

2. Data for the Trapezium, the Pleiades and M35 open clusters (Bouvier et al. 1998; Barrado y Navascúes et al. 2000), and the field (Reid et al. 1999) are consistent with the same IMF; this mass function is flat or slowly rising from the brown dwarf regime to 0.6–1.0 $M_\odot$, where it rolls over to a power law with a slope of ~ 1.7, similar to or slightly steeper than the Salpeter value of 1.35. The similarity of these mass functions is consistent with the suggestion that members of the field have formed predominantly in clusters.

3. Whereas the IMF that characterizes young clusters and the field rolls over near 0.8 $M_\odot$ and is not log-normal, recent studies have found that the IMFs of globular clusters peak near 0.3 $M_\odot$ and can be described by a log-normal function (Paresce & De Marchi 1999). As a result, there appear to be fundamental differences in the IMF between globular clusters and Galactic disk clusters.

4. Using the high spatial resolution and sensitivity of NICMOS images, we have penetrated the bright nebulosity of the Trapezium and identified a population of ~ 50 likely brown dwarfs, where the least massive candidate is ~ 0.01 $M_\odot$ if the median age of the Trapezium is assumed. Most theories of the IMF do not predict the formation of free-floating objects in significant numbers at such low masses. For instance, this low-mass population rules out a log-normal IMF in this cluster, contrary to some theories of star formation.

M. McCaughrean kindly provided unpublished K-band photometry. We are grateful to F. Allard, I. Baraffe, and F. D'Antona for access to their most recent calculations and thank E. Bergin, F. D'Antona, B. Elmegreen, and P. Myers for helpful discussions. Comments on the manuscript by J. Stauffer and B. Wilking are appreciated. K. L. was funded by a postdoctoral fellowship at the Harvard-Smithsonian Center for Astrophysics. Portions of this work were supported by NASA grant NAGW-4083 under the Origins of Solar Systems program. Support for this work was also provided through NASA grant NAG5-3042 to the Nichmos IDT.

APPENDIX A

METHOD OF CLASSIFICATION

K-band spectral classification of young stars has been performed for L1495E, IC 348, and ρ Oph, as described in detail by LR98, LRLL, and LR99. However, the classification of the Trapezium sample is more difficult than in the previous studies because of the combination of low spectral resolution ($R = 800$) and bright nebular emission from the Orion Nebula. The K-band absorption lines that appear at this resolution are Brγ (2.166 μm), Na (2.206, 2.209 μm), Ca (2.161, 2.163, 2.166 μm), and CO (2.294, 2.323, 2.353, 2.383 μm), while weaker lines of Mg (2.281 μm) and Mg and Al (2.11 μm) can sometimes be detected (LRLL). At a slightly higher resolution ($R = 1200$), Mg and Al and several other metal lines can be measured accurately, providing better constraints on the spectral type and continuum veiling (LR99), where the veiling at 2.2 μm is defined as $r_K = I_{2.2}(\text{IR excess})/I_{2.2}(\text{star})$. The brightest transitions of H I and H_2 in the Orion Nebula (Luhman, Engelbracht, & Luhman 1998) fall near the photospheric absorption lines of Brγ, Mg/Al at 2.11 μm, and several weaker metal lines between Na and Ca. Because the nebular emission varies on small scales, we could not accurately subtract the emission lines from the stellar spectrum. Thus, we have useful measurements of only Na, Ca, and CO. Because of the anticorrelation of Brγ with the metal lines, it is an important line in the classification of G and early K stars, and its loss makes more difficult distinguishing these stars from heavily veiled M stars.

To classify the Trapezium stars, we compared each K-band spectrum to the others in the sample and organized most of the data into groups of spectra that appeared the same within the noise. The spectra in each group were then combined into a spectrum representative of that group. The composite spectra from the 14 groups are given in Figure 3 along with data for the BN object and source n. Wavelengths near H_2 1–0 S(1) (2.122 μm) and Brγ (2.166 μm) are not plotted because of contamination from nebular emission, except for BN, which is much brighter than the surrounding emission. The composite spectra were classified by comparison to dwarf standards from LR98 with various amounts of artificial veiling, and the resulting classification was assigned to each star included in that composite. After deriving a spectral type for each star, we calculated the percentage increase in the strength of the CO absorption over that of the standard dwarf of that type. The IR spectral types, veilings, and CO absorption strengths are listed in Figure 3 and Table 1. Spectra with very low signal-to-noise were not included in the composite spectra and have no IR classification. A few stars exhibited steam absorption indicative of mid-to-late M types and were classified individually rather than combined into composites.

We adopted previously measured optical spectral types when available. Otherwise, we used the IR classifications. For stars that have both IR and optical spectra, the two spectral types generally agree with within the uncertainties. This comparison is an important check of the IR classifications since the Trapezium stars are extremely young and show significant departures

from dwarfs in their K-band spectra, as we illustrate in § 2.2.3. The optical classifications can also differ substantially among themselves; in these cases we adopted the optical type that was most consistent with the IR data. For stars with uncertain IR spectral types and no optical data, we adopted the average type for the optically classified objects with the same IR spectrum. An example is source 207, which is classified as $\geq$G6 in the IR. Objects 257 and 266 have very similar IR spectra to 207 and have optical types of K0–K6 and G8–K2, hence we adopted K0–K6 for 207. For object 114, the IR type is K4–M2. However, since the other five stars with the same IR spectra have spectral types covering a smaller range, K7–M2, we take this as the classification for 114. Object 119 is a binary system where the components have optical spectral types of B5–B8 and G0–G5. At the spectral resolution of our K-band data, the B star should be featureless in the K-band except for Brγ absorption. Hence, our spectrum of this unresolved system indicates a spectral type of G or K with continuum veiling, which arises from the B star rather than an IR excess in this case. For object 133, we find that the K-band spectrum implies a spectral type of K0–K7, whereas Hillenbrand (1997) reports an optical type of F2–F7. Spectra from two different nights confirm that we observed the correct star. We adopt the IR classification for this object, although it could be binary system where an F primary and a K secondary dominate in the optical and IR, respectively, similar to source 133.

APPENDIX B

COLORS AND EXTINCTIONS

To measure reddenings for the sources in Table 1, we examine the various optical and IR colors that are available. We then determine the reddening relation and intrinsic stellar colors for the NICMOS bands. Standard dwarf colors are taken from the compilation of Kenyon & Hartmann (1995) for types earlier than M0 and from the young disk populations described by Leggett (1992) for types of M0 and later.

The color excesses $E(V-I_C)$, $E(I_C-K)$, and $E(I_C-m_{160})$ have been computed for stars with spectral types by assuming the intrinsic colors are those of standard dwarfs. The correlations among these excesses and $m_{110}-m_{160}$ are then examined. Several anomalous sources are very red in $V-I_C$ relative to $m_{110}-m_{160}$ and I_C-m_{160}, which is likely a result of cool companions. In addition, $V-I_C$ is prone to contamination from star spots and the derived extinction is sensitive to errors in spectral type for M stars (Gullbring et al. 1998). The $E(I_C-K)$ excess and other colors associated with K are systematically redder for a portion of the sample, suggesting the presence of IR excess emission at K. We find that the best reddening determination uses the I_C-m_{160} color, providing a long wavelength baseline for measuring reddening while remaining relatively free of short or long wavelength excess emission. One disadvantage of this color is that the two bands were measured at different epochs and variability will increase the uncertainty in the color. We note that the colors I_C-J, I_C-H, and I_C-K may differ from the dwarf colors for young cool sources (Luhman 1999), in which case I_C-m_{160} would not be the ideal color for estimating reddening. However, this is not a problem here since there are few late M objects in our spectroscopic sample. For effective wavelengths of 8100 Å (for M stars), 1.60 μm, and 1.65 μm for I_C, m_{160}, and H, respectively, the extinction law of Rieke & Lebofsky (1985) gives reddening relations of $A_I = 3.32A_H$, $A_{160} = 1.06A_H$, and $A_H = E(I_C-m_{160})/2.26$. For sources lacking I_C, reddenings are measured from $m_{110}-m_{160}$ with the extinction relations and intrinsic colors derived below. Saturated stars in the NICMOS images are dereddened to the standard dwarf values of $V-I_C$ with $A_H = E(V-I_C)/2.23$. The reddenings in Table 1 are computed for the average spectral types of the adopted ranges.

As extinction increases, the effective wavelengths of the NICMOS band passes, particularly the very wide F160W, shift to longer wavelengths. We simulated the change in $m_{110}-m_{160}$ as a function of reddening from $A_H = 0$ to 4 assuming uniform transmissions for the F110W (0.8–1.4 μm) and F160W (1.4–1.8 μm) filters and adopted the functional form of the reddening law found in Cardelli, Clayton, & Mathis (1989). The results of such modeling are independent of R_V for bands longward of V. The simulated reddening relation does depend on the shape of the intrinsic stellar spectrum, although the effect is only noticeable at large extinctions. For instance, a reddening of $A_H = 1.4$ leads to $E(m_{110}-m_{160}) = 1.20$, 1.30, and 1.41 for effective temperatures of 3000, 4000, and 6000 K, where a synthetic spectrum of Allard et al. (1998) was used for 3000 K and blackbodies were assumed for 4000 and 6000 K. As shown in the color-magnitude diagram in Figure 5, most sources in the NICMOS data have reddenings of $A_H \lesssim 1.4$, thus the reddening relation for $T_{\rm eff} = 4000$ K should be sufficient for all sources. In Figure 13, this reddening vector is plotted with $m_{160}-K$ versus $m_{110}-m_{160}$ using the K-band data of MS for the central square arcminute of the Trapezium. The simulated colors redden more slowly with additional extinction in a manner consistent with the reddening vector implied by the embedded stars in Figure 13.

The origin of a reddening vector in Figure 13 will correspond to the intrinsic colors of a given star, or star-disk system in the case of a classical T Tauri star. One example of such a vector is shown. After dereddening $m_{110}-m_{160}$ with extinctions derived from $E(I_C-m_{160})$, we find intrinsic NICMOS colors of 0.8 ± 0.3 independent of K and M spectral types. The large scatter in this dereddened color is not surprising considering the observational errors in $m_{110}-m_{160}$ and the uncertainties in the $E(I_C-m_{160})$ reddening from possible variability between measurements of I_C and m_{160}. The intrinsic NICMOS colors of these young stars can also be estimated by examining the locus of sources in Figure 5. A large number of stars have colors of $m_{110}-m_{160} = 1$–1.4. If these are the least reddened objects in the cluster and if the Trapezium has a minimum extinction of $A_V \sim 2.4$ (Herbig & Terndrup 1986), then an intrinsic color of $\sim$0.8 is again implied. The blue boundary of the locus in Figure 5 is fairly constant for all magnitudes shown, supporting the notion that $m_{110}-m_{160}$ does not depend significantly on spectral type. Assuming an intrinsic color of 0.8, the simulated reddening relation for a star of $T_{\rm eff} = 4000$ K is $A_H = -0.546 + 0.550(m_{110}-m_{160}) + 0.179(m_{110}-m_{160})^2$.

Several close pairs in the optical *HST* images of Prosser et al. (1994) are unresolved in the other data. For these systems, we combined the optical photometry of the two components and treated them as one object. When $V-I_C$ was not available for

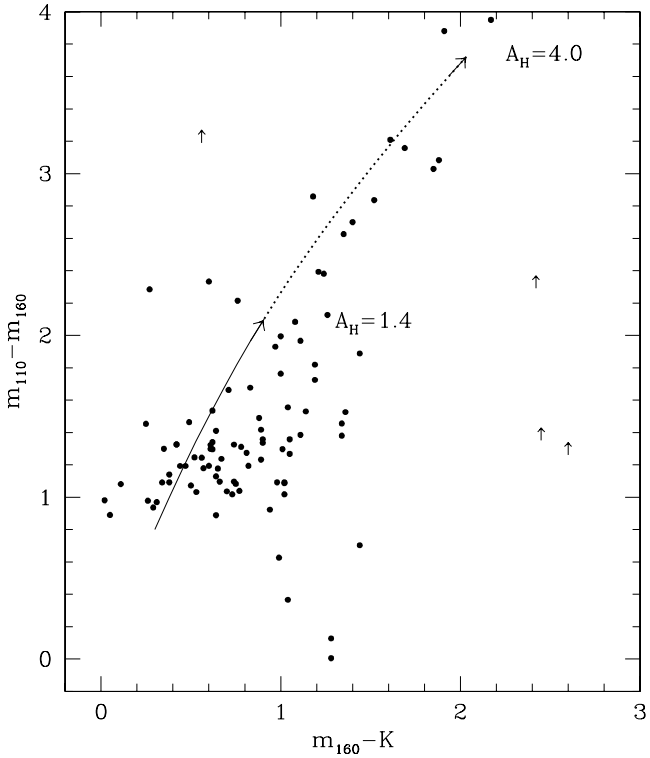

FIG. 13.—$m_{160}-K$ vs. $m_{110}-m_{160}$ for stars within K-band images of the central square arcminute of the Trapezium Cluster (MS). Variability between the K-band and NICMOS observations is likely for some of these young stars, accounting for some of the scatter in $m_{160}-K$.

one component, $V-I_C$ for the other star was adopted for the system. The optical data for ID 488a assigned to 123 in Table 1 probably applies to both 116 and 123. Since we have no V or NICMOS data for these two stars, the reddening is measured by assuming that each star has the I_C-K color of the composite system. The optical photometry for ID 524 also applies to both 165 and 169. Extinctions were computed from the NICMOS colors for these two stars. The extinction for object 49 was estimated with I_C-K, the only color available.

REFERENCES

Abt, H. A., & Levato, H. 1977, PASP, 89, 797
Adams, F. C., & Fatuzzo, M. 1996, ApJ, 464, 256
Ali, B., & DePoy, D. L. 1995, AJ, 109, 709
Allard, F., Alexander, D. R., & Hauschildt, P. H. 1998, in ASP Conf. Ser. 154, The Tenth Cambridge Workshop on Cool Stars, Stellar Systems, and the Sun, ed. R. A. Donahue & J. A. Bookbinder (San Francisco: ASP), 63
Baraffe, I., Chabrier, G., Allard, F., & Hauschildt, P. H. 1998, A&A, 337, 403 (B98)
Barrado y Navascúes, D., Stauffer, J. R., Bouvier, J., & Martín, E. L. 2000, ApJ, submitted
Becklin, E. E., & Neugebauer, G. 1967, ApJ, 147, L799
Bernasconi, P. A. 1996, A&AS, 120, 57
Biscaya Holzbach, A., Rieke, G. H., Calvet, N., Luhman, K. L., & Hanson, M. M. 2000, ApJ, submitted
Bonnell, I. A., Bate, M. R., Clarke, C. J., & Pringle, J. E. 1997, MNRAS, 285, 201
Bouvier, J., Stauffer, J. R., Martín, E. L., Barrado y Navascués, D., Wallace, B., & Bejar, V. J. S. 1998, A&A, 336, 490
Burrows, A., Marley, M., Hubbard, W. B., Lunine, J. I., Guillot, T., Saumon, D., Freedman, R., Sudarsky, D., & Sharp, C. 1997, ApJ, 491, 856
Calvet, N., Patiño, A., Magris C., G., & D'Alessio, P. 1991, ApJ, 380, 617
Cardelli, J. A., Clayton, G. C., & Mathis, J. S. 1989, ApJ, 345, 245
Cohen, M., & Kuhi, L. V. 1979, ApJS, 41, 743
Comerón, F., Rieke, G. H., & Neuhäuser, R. 1999, A&A, 343, 477
Comerón, F., Rieke, G. H., & Rieke, M. J. 1996, ApJ, 473, 294
D'Antona, F., & Mazzitelli, I. 1994, ApJS, 90, 467
———. 1997, Mem. Soc. Astron. Italiana, 68, 807 (DM97)
Edwards, S., et al. 1993, AJ, 106, 372
Elmegreen, B. G. 1997, ApJ, 486, 944
———. 1999a, ApJ, 515, 323
———. 1999b, in Unsolved Problems in Stellar Evolution, ed. M. Livio (Cambridge: Cambridge Univ. Press)
Genzel, R., & Stutzki, J. 1989, ARA&A, 27, 41
Goldsmith, P. F., Bergin, E. A., & Lis, D. C. 1997, ApJ, 491, 615
Gould, A., Bahcall, J. N., & Flynn, C. 1997, ApJ, 482, 913
Greene, T. P., & Lada, C. J. 1997, AJ, 114, 2157
Greene, T. P., & Meyer, M. R. 1995, ApJ, 450, 233
Gullbring, E., Hartmann, L., Briceño, C., & Calvet, N. 1998, ApJ, 492, 323
Hamilton, C. 1994, Masters thesis, Wesleyan University
Hawley, S. L., Tourtellot, J. G., & Neill, R. I. 1999, AJ, 117, 1341
Henriksen, R. N. 1986, ApJ, 310, 189
———. 1991, ApJ, 377, 500
Herbig, G. H. 1998, ApJ, 497, 736
Herbig, G. H., & Terndrup, D. M. 1986, ApJ, 307, 609
Hillenbrand, L. A. 1997, AJ, 113, 1733
Hillenbrand, L. A., & Carpenter, J. M. 2000, ApJ, 540, 236
Hillenbrand, L. A., & Hartmann, L. W. 1998, ApJ, 492, 540
Hunter, D. A., Light, R. M., Holtzman, J. A., Lynds, R., O'Neil, E. J., Jr., & Grillmair, C. J. 1997, ApJ, 478, 124
Johnson, H. L. 1965, ApJ, 142, 964
Jones, B. F., & Walker, M. F. 1988, AJ, 95, 1755
Kenyon, S. J., & Hartmann, L. 1995, ApJS, 101, 117
Kleinmann, S. G., & Hall, D. N. B. 1986, ApJS, 62, 501
Kleinmann, D. E., & Low, F. J. 1967, ApJ, 149, L1
Klessen, R. S., Burkert, A., & Bate, M. R. 1998, ApJ, 501, L205
Kroupa, P. 1995a, ApJ, 453, 350
———. 1995b, ApJ, 453, 358
Kruegel, E., & Siebenmorgen, R. 1995, A&A, 288, 929
Lada, E. A., Strom, K. M., & Myers, P. C. 1993, in Protostars and Planets III, eds. E. H. Levy, J. I. Lunine, & M. S. Matthews (University of Arizona Press, Tucson), 245
Larson, R. B. 1992, MNRAS, 256, 641
Leggett, S. K. 1992, ApJS, 82, 351
Leggett, S. K., Allard, F., Berriman, G., Dahn, C. C., & Hauschildt, P. H. 1996, ApJS, 104, 117
Lejeune, C., & Bastien, P. 1986, ApJ, 309, 167
Levato, H., & Abt, H. A. 1976, PASP, 88, 712
Lonsdale, C. J., Becklin, E. E., Lee, T. J., & Stewart, J. M. 1982, AJ, 87, 1819
Luhman, K. L. 1999, ApJ, 525, 466
———. 2000, ApJ, submitted

Luhman, K. L., Engelbracht, C. W., & Luhman, M. L. 1998, ApJ, 499, 799
Luhman, K. L., & Rieke, G. H. 1998, ApJ, 497, 354 (LR98)
———. 1999, ApJ, 525, 440 (LR99)
Luhman, K. L., Rieke, G. H., Lada, C. J., & Lada, E. A. 1998, ApJ, 508, 347 (LRLL)
Massey, P., & Hunter, D. A. 1998, ApJ, 493, 180
McCaughrean, M. J., & Stauffer, J. R. 1994, AJ, 108, 1382 (MS)
McLeod, B. 1997, in The 1997 *HST* Calibration Workshop, eds. S. Casertano, R. Jedrzejewski, C. D. Keyes, & M. Stevens (Baltimore, MD: STScI), 281
Menten, K. M., & Reid, M. J. 1995, ApJ, 445, L157
Meyer, M. R., Calvet, N., & Hillenbrand, L. A. 1997, AJ, 114, 288
Miller, G. E., & Scalo, J. M. 1979, ApJS, 41, 513
Motte, F., André, P., & Neri, R. 1998, A&A, 336, 150
Murray, S. J., & Lin, D. N. C. 1996, ApJ, 467, 728
Myers, P. C. 1998, ApJ, 496, L109
Parenago, P. P. 1954, Trudy Sternberg Astron. Inst., 25
Paresce, F., & De Marchi, G. 2000, ApJ, in press
Petr, M. G., Coudé Du Foresto, V., Beckwith, S. V. W., Richichi, A., & McCaughrean, M. J. 1998, ApJ, 500, 825
Price, N. M., & Podsiadlowski, Ph. 1995, MNRAS, 273, 1041
Prosser, C. F., Stauffer, J. R., Hartmann, L., Soderblom, D. R., Jones, B. F., Werner, M. W., & McCaughrean, M. J. 1994, ApJ, 421, 517
Reid, I. N., & Gizis, J. E. 1997, AJ, 113, 2246
Reid, I. N., et al. 1999, ApJ, 521, 613
Rieke, G. H., & Lebofsky, M. J. 1985, ApJ, 288, 618
Salpeter, E. E. 1955, ApJ, 121, 161
Samuel, A. E. 1993, Ph. D. thesis, Australian National Univ.
Scalo, J. 1986, Fundam. Cosmic Phys., 11, 1
———. 1998, in ASP Conf. Ser. 142, The Stellar Initial Mass Function Proceedings, ed. G. Gilmore & D. Howell (San Francisco: ASP), 201
Scalo, J. 2000, in The Birth of Galaxies, ed B. Guiderdoni et al. (Gif-sur-Yvette, Editions Frontières), in press
Schmidt-Kaler, T. 1982, in Landolt-Bornstein, Group VI, Vol. 2, ed. K.-H. Hellwege (Berlin: Springer), 454
Scholz, R.-D., et al. 1999, A&AS, 137, 305
Shu, F. H., Adams, F. C., & Lizano, S. 1987, ARA&A, 25, 23
Silk, J. 1995, ApJ, 438, 41
Simon, M., Close, L. M., & Beck, T. L. 1999, ApJ, 117, 1375
Sirianni, M., Nota, A., Leitherer, C., De Marchi, G., & Clampin, M. 2000, ApJ, 533, 203
Strand, K. Aa. 1958, ApJ, 128, 114
Testi, L., & Sargent, A. I. 1998, ApJ, 508, L91
Trumpler, R. J. 1931, PASP, 43, 255
van Altena, W. F., Lee, J. T., Lee, J. F., Lu, P. K., & Upgren, A. R. 1988, AJ, 95, 1744
Umemoto, T., Kamazaki, T., Sunada, K., Kitamura, Y., & Hasegawa, T. 2000, in 33rd ESLAB Symp., Star Formation from the Small to the Large Scale, ed. A. Wilson (Noordwijk: ESO), in press
White, R. J., Ghez, A. M., Reid, I. N., & Schultz, G. 1999, ApJ, 520, 811
Williams, D. M., Comerón, F., Rieke, G. H., Rieke, M. J. 1995, ApJ, 454, 144
Williams, D., Thompson, C. L., Rieke, G. H, & Montgomery, E. F. 1993, Proc. SPIE, 1308, 482
Zapatero Osorio, M. R., Béjar, V. J. S., Rebolo, R., Martín, E. L., & Basri, G. 1999, ApJ, 524, L115
Zapatero Osorio, M. R., et al. 2000, Science, submitted
Zoccali, M., Cassisi, S., Frogel, J. A., Gould, A., Ortolani, S., Renzini, A., Rich, R. M., & Stephens, A. W. 2000, ApJ, 530, 418